CDK4 or CDK6 upregulation induces DNA replication stress and genomic instability to cause EGFR targeted therapy resistance in lung cancer

Beatrice Gini[1,2*], Philippe Gui[1,2], Wei Wu[1,2], D. Lucas Kerr[1,2], Lisa Tan[1,2], Dora Barbosa[1,2], Victor Olivas[1,2], Paul Allegakoen[1,2], Carlos Gomez[1,2], Patrick R. Halliday[1], Sarah Elmes[2], Veronica Steri[2], Turja Chakrabarti[1,2], Trever G. Bivona[1,2,3 *], Collin M. Blakely[1,2 *]

Author Affiliations

1 Department of Medicine, University of California, San Francisco, San Francisco, CA 94158, USA.

2 Helen Diller Family Comprehensive Cancer Center, University of California, San Francisco, San Francisco, CA 94158, USA.

3 Chan-Zuckerberg Biohub, San Francisco, CA 94158, USA.

*co-corresponding authors

Email: collin.blakely@ucsf.edu or trever.bivona@ucsf.edu

Conflicts of Interest: C.M.B receives research funding from AstraZeneca, Novartis, Roche, and Puma.

Abstract

Epidermal growth factor receptor (EGFR)–mutant lung adenocarcinomas (LUAD) harbor a complex landscape of genetic co-alterations and potential oncogenic interactions. Among them are recurrent amplifications of the cell cycle regulatory genes *CDK4* and *CDK6*, which have been clinically implicated in resistance to EGFR tyrosine kinase inhibitors (TKIs). However, the mechanisms by which CDK4/6 upregulation promotes therapy resistance remain poorly defined. Here, we demonstrate that CDK4 or CDK6 overexpression limits EGFR inhibitor-induced proliferative arrest, promoting continued cell cycle progression. This is accompanied by elevated replication stress, increased TPX2 expression, DNA damage leading to ATM activation, and ultimately genomic instability. Integrative transcriptomic and copy number analyses of EGFR-mutant LUAD tumors from both patients and preclinical models revealed that *CDK4* or *CDK6* amplification is associated with the upregulation of genes linked to tumor progression, including *AGR2*, *ASNS*, and *STEAP1*. *CDK4* amplification was also highly correlated with gene expression changes associated with epithelial-to-mesenchymal transition (EMT) in a single-cell RNA sequencing dataset from patient biopsies. In preclinical models, co-treatment with CDK4/6 and EGFR inhibitors restored proliferative arrest, induced tumor cell apoptosis, and reduced replication stress, DNA damage, and genomic instability. Our findings uncover a mechanistic basis for EGFR inhibitor resistance of *CDK4* and *CDK6* amplified EGFR-mutant LUAD. They also provide a rationale for the biomarker-driven clinical development of combination EGFR and CDK4/6-targeted therapies for the treatment of a subset of EGFR-mutant LUAD patients.

45 **Main Text**

46 Targetable oncogenic driver mutations are identifiable in the majority of LUADs (1).
47 Oncogenic activating mutations (EGFR-mutant) are present in ~ 15-30% of patients in the U.S.
48 and more than 50% of cases in Asia (2-4). Small molecule EGFR tyrosine kinase inhibitors (TKIs),
49 including erlotinib, gefitinib, afatinib, dacomitinib, and third-generation EGFR inhibitors
50 osimertinib and lazertinib, improve overall response (ORR) rate as well as progression-free
51 survival (PFS) compared to traditional cytotoxic chemotherapy. However, TKI resistance limits
52 the effectiveness of these therapies after approximately one to two years in patients with metastatic
53 disease (5-8). Several mechanisms of acquired resistance to EGFR TKIs have been identified,
54 including on-target mutations within *EGFR*, amplification of other receptor tyrosine kinases
55 (RTKs), such as *MET*, oncogenic fusions involving *ALK* and *RET*, as well as activating mutations
56 within the MAPK signaling pathway (9). Recent data indicate a role for genes that regulate cell
57 cycle progression, including *CDK4* and *CDK6,* in EGFR TKI resistance (10-12).

58 Analysis of circulating tumor DNA (ctDNA) from a large cohort of advanced-stage EGFR-
59 mutant LUAD patients identified co-alterations in cell cycle regulatory genes in a significant
60 proportion of cases, which was associated with decreased response rate to osimertinib, as well as
61 reduced PFS and overall survival (OS) (10). Among the cell cycle regulatory genes, *CDK4* and
62 *CDK6* copy number alterations (CNAs; amplifications) were most closely associated with
63 decreased PFS and decreased responsiveness to osimertinib treatment (10). The role of CDK4 and
64 CDK6 in limiting osimertinib responsiveness has also emerged in preclinical studies (13-15).
65 Recent clinical data further support the role of *CDK4* and *CDK6* gene alterations in *de novo* EGFR
66 TKI resistance in EGFR-mutant LUAD patients (12,16). However, the mechanism(s) underlying
67 these effects are incompletely defined.

68 CDK4 and CDK6 proteins regulate G1/S cell cycle progression through phosphorylation
69 of retinoblastoma protein 1 (Rb). Phosphorylation of Rb releases its inhibitory binding to
70 transcription factor family E2F, which mediates the transition from G1 to S-phase of the cell cycle
71 (17). While CDK4 and CDK6 have been established to limit response to oncogenic EGFR
72 inhibition in lung cancer preclinical models and in patients, the functional characterization of the
73 impact of CDK4/6 upregulation on TKI resistance and the mechanism(s) underlying these effects
74 have not been clearly defined beyond an association with changes in Rb phosphorylation and the
75 G1/S cell cycle transition. Alterations in cell cycle genes have been shown to induce deregulation
76 of cell cycle checkpoints, compromising DNA integrity and contributing to the accumulation of
77 DNA damage and abnormal chromosomal segregation (18-20). Here, we provide evidence that
78 CDK4 or CDK6 upregulation induces DNA replication stress and genomic instability in EGFR-
79 mutant LUAD, activating TPX2 and ATM, which are known to promote EGFR TKI resistance
80 (21,22). In addition, we identified recurrent copy-number changes associated with CDK4 and
81 CDK6 upregulation and increased expression of genes related to EMT, which may also contribute
82 to tumor progression. Co-treatment with a CDK4/6 inhibitor reversed many of these effects and
83 re-sensitized EGFR-mutant LUAD to EGFR TKI treatment in both *in vitro* and *in vivo* patient-
84 derived models. These findings provide novel mechanistic and therapeutic insights into EGFR-
85 mutant LUAD.
86
87 **Results**
88 **CDK4 and CDK6 upregulation promote sustained DNA synthesis and cell cycle progression**
89 **during EGFR inhibition in EGFR-mutant LUAD.**

90 To investigate the mechanism(s) by which CDK4 or CDK6 may promote decreased
91 responsiveness of EGFR-mutant lung cancer cells to EGFR TKI treatment, we utilized patient-
92 derived EGFR-mutant LUAD cell lines: H1975 ($EGFR^{L858R/T790M}$, $CDK4/6^{wt}$) and PC9
93 ($EGFR^{del19}$, $CDK4/6^{wt}$); a primary, patient-derived organoid (PDO), TH107 ($EGFR^{del19}$,
94 $CDK4/6^{wt}$); and a patient-derived xenograft (PDX), TH116 ($EGFR^{L858R}$, $CDK4^{wt}$, $CDK6^{AMP}$)
95 (Supplementary Tables 1-2). We overexpressed CDK4 or CDK6 in H1975 and PC9 EGFR-mutant
96 LUAD cells (Supplementary Fig. 1A-D) and quantified protein expression. This demonstrated a
97 similar degree of CDK4 overexpression observed in HCC827 ($EGFR^{del19}$, $CDK4^{AMP}$, $CDK6^{wt}$)
98 cells with endogenous *CDK4* amplification and CDK6 overexpression to a similar degree observed
99 in the TH116 PDX ($EGFR^{L858R}$, $CDK4^{wt}$, $CDK6^{AMP}$) (Supplementary Fig. 1E-J), indicating a
100 pathophysiology-relevant degree of protein overexpression. CDK4 and CDK6 overexpressing PC9
101 and H1975 cells demonstrated relative resistance to osimertinib in colony formation assays
102 (Supplementary Fig. 2). TH107 ($EGFR^{del19}$, $CDK4/6^{wt}$) PDOs, which had no evidence of *CDK4*
103 or *CDK6* CNAs (Supplementary Fig. 3A, B), were genetically engineered to overexpress CDK4
104 or CDK6 through lentiviral infection to model *CDK4/6* CNAs (Supplementary Fig. 3C) (23). This
105 resulted in decreased responsiveness to osimertinib treatment in multiple assays (Supplementary
106 Fig. 3D-H). These results confirm that CDK4 or CDK6 overexpression results in relative resistance
107 to the EGFR TKI osimertinib in multiple preclinical models of EGFR-mutant LUAD.
108 To assess the effects of CDK4 or CDK6 overexpression on EGFR signaling in the context
109 of TKI treatment *in vivo*, we assessed how an osimertinib dose range modulates EGFR
110 phosphorylation and signaling in CDK4 or CDK6-overexpressing H1975 CDXs (Fig. 1A).
111 Osimertinib (at 5 mg/kg/day) was sufficient to inhibit EGFR signaling in E.V. control and CDK4
112 or CDK6 overexpressing CDXs (Fig. 1A, B). However, CDK4 or CDK6 overexpression conferred

113 relative resistance to osimertinib treatment compared to E.V. control H1975 CDXs (Fig. 1C, D
114 and Supplementary Fig. 4) and in CDK6 overexpressing PC9 CDXs (Supplementary Fig. 5).

115 To assess which downstream pathways may be affected by CDK4 and CDK6 activation,
116 we evaluated gene expression changes in CDK4 and CDK6-overexpressing CDXs compared to
117 controls. Gene set enrichment analysis (GSEA) of CDK4 or CDK6 overexpressing H1975 CDXs
118 showed significant upregulation of E2F1 target genes, which mediate G1/S transition (17),
119 together with substantial enrichment of G2/M checkpoint, HALLMARK_MYC_TARGETS_V1,
120 and DNA repair genes (Fig. 1E and Supplementary Fig. 6A-D). These data suggest that EGFR-
121 mutant LUAD CDXs overexpressing CDK4 or CDK6 upregulate the E2F1 transcriptional
122 program, which promotes G1/S transition, entry in the S-phase of the cell cycle, and proliferation
123 (17,24).

124 We further evaluated this by quantifying the expression of the proliferation biomarker Ki-
125 67, which was significantly higher in the CDK4 and CDK6 overexpressing tumor xenografts
126 versus controls, and was maintained upon treatment with osimertinib (Fig. 1F-H). The quantity of
127 newly synthesized DNA, measured by quantifying EdU incorporation in CDK4 and CDK6
128 overexpressing tumor xenografts, was also increased compared to controls in both vehicle and
129 osimertinib treatment groups (Supplementary Fig. 7A-C). These data demonstrate that
130 overexpression of CDK4 or CDK6 results in increased DNA synthesis and cellular proliferation
131 maintained during osimertinib treatment.

132

133 **CDK4 and CDK6 upregulation lead to DNA replication stress in EGFR-mutant LUAD.**

134 We hypothesized that increased DNA synthesis and proliferation observed in *in vivo*
135 models could lead to DNA replication stress and potentially replication stress-associated DNA

136 damage in CDK4 and CDK6-overexpressing LUADs. We evaluated biomarkers indicative of
137 DNA replication stress and DNA damage repair (DDR) (25,26), including the phosphorylation of
138 Rb protein, expression of TPX2, a microtubule nucleation factor, and phosphorylation of
139 replication protein A (RPA). CDK4 and CDK6-expressing CDXs demonstrated higher expression
140 levels of these DNA replication stress biomarkers than controls (Fig. 1I, J, and Supplementary Fig.
141 7D, E).

142 Given the role of TPX2 during interphase as a protective factor of DNA fork stability
143 during replication stress (26) and its role in EGFR TKI resistance (22), we assessed the nuclear
144 expression of TPX2 in CDK4 and CDK6-overexpressing H1975 CDXs by immunohistochemistry.
145 We identified increased TPX2 nuclear expression compared to controls (Supplementary Fig. 7F,
146 G). Increased TPX2 nuclear localization in CDK4 and CDK6 overexpressing CDXs was also
147 observed post-osimertinib treatment, although it was decreased compared with pre-treatment
148 levels (Supplementary Fig. 7F, G). *TPX2* gene expression has been shown to depend on the activity
149 of transcription factor E2F1 (26). E2F1 knockdown resulted in the downregulation of *TPX2* in
150 EGFR-mutant NSCLC cells (Supplementary Fig. 7H, I). Together, these results demonstrate that
151 CDK4 and CDK6 overexpression induce biomarkers of DNA replication stress in EGFR-mutant
152 lung cancer *in vivo* models.

153 DNA replication stress can also induce DNA damage and activation of DNA damage
154 response (DDR) pathways, as the G1/S checkpoint is necessary to ensure cellular repair of DNA
155 damage before DNA replication (27). We assessed phosphorylation of ataxia-telangiectasia
156 mutated (ATM) as a DDR biomarker and known promoter of EGFR TKI resistance (21), as well
157 as γ-H2AX and EdU double immunofluorescence staining in CDK4 and CDK6 overexpressing
158 tumor xenografts as a marker of DNA damage in proliferating cells. CDK4 and CDK6-

159 overexpressing CDXs demonstrated increased expression of phosphorylated ATM (Fig. 1I, J),
160 indicative of DDR activation. Further analysis of RNA sequencing data obtained from CDK4 and
161 CDK6 overexpressing H1975 CDXs revealed evidence of significant upregulation of key DDR
162 inducers and effectors, including *CHEK1*, *CHEK2*, and *RAD51* (Fig. 2A, B), supporting this
163 hypothesis. CDK4 and CDK6-overexpressing H1975 CDXs also showed significantly higher
164 γH2AX foci in proliferating cells than controls (Fig. 2C, D). This effect persisted during
165 osimertinib treatment in CDK4 and CDK6 overexpressing tumors (Fig. 2E, F). These data
166 highlight the accumulation of DNA replication stress and damage upon CDK4 and CDK6
167 upregulation, which persist upon osimertinib treatment in EGFR-mutant LUAD cells.
168

169 **CDK4 and CDK6 upregulation increases genomic instability and the acquisition of tumor-**
170 **promoting CNAs in EGFR-mutant LUAD.**

171 Given the replication stress and DNA damage observed upon CDK4 and CDK6
172 upregulation in preclinical models, we investigated whether CDK4 or CDK6 amplification or
173 overexpression drives genomic instability in EGFR-mutant LUAD. As a measure of genomic
174 instability, we assessed the fraction of genome altered (FGA) using whole-exome sequencing of
175 CDK4- and CDK6-overexpressing EGFR-mutant NSCLC CDXs treated with either vehicle or
176 osimertinib. We observed a 15- to 20-fold increase in FGA in CDK4 and CDK6-overexpressing
177 tumors compared to E.V. controls under both conditions (Fig. 3A), suggesting that CDK4 or CDK6
178 up-regulation increases genomic instability. Despite the elevated structural GIN, tumor mutation
179 burden (TMB) remained unchanged across CDK4, CDK6, and E.V. xenografts in both vehicle and
180 osimertinib treatment arms, as determined by SNV analysis (Supplementary Fig. 8A, B),
181 suggesting that CDK4/6-associated genomic instability primarily involves copy number

182 alterations rather than increased point mutations. Integration of RNA-seq with CNA data revealed
183 a subset of genes demonstrating both CN gains and transcriptional upregulation in CDK4 (Fig.
184 3B) and CDK6 (Fig. 3C) overexpressing CDXs. Several known pro-tumor effectors, including
185 *AGR2*, *CBX3*, *ANLN*, *SEC61G*, *PSMA2*, *STEAP1*, and *GGCT,* were significantly upregulated at
186 both the DNA and RNA levels in both CDK4 and CDK6 overexpression CDXs (Fig. 3B-E) (27-
187 34). Notably, these overlapping CNA and RNA expression signatures persisted upon osimertinib
188 treatment (Fig. 3F), suggesting that upregulation of these genes may play a role in EGFR TKI
189 resistance. Gene ontology and pathway enrichment analysis of the overlapping genes revealed
190 strong enrichment for pathways involved in cell cycle regulation, DNA replication, and DNA
191 repair, consistent with the role of CDK4 and CDK6 in driving proliferation and managing
192 replication stress-induced DNA damage (Supplementary Fig. 8C, D). These results indicate that
193 CDK4 and CDK6 upregulation is associated with increased FGA and transcriptional activation of
194 DNA repair and cell cycle regulatory genes, which may contribute to genomic instability and
195 resistance to EGFR inhibition.
196
197 **CDK4 and CDK6 inhibition reduces DNA replication stress and genomic instability in**
198 **CDK4/6 upregulated EGFR-mutant CDXs and PDXs.**
199 Combination therapy with osimertinib and the CDK4/6 inhibitor palbociclib has been
200 shown to inhibit Rb phosphorylation, induce cell cycle arrest, and decrease tumor cell survival in
201 EGFR-mutant cell lines (15). Similarly, we found that combination treatment with osimertinib and
202 palbociclib was sufficient to induce regression of CDK4 or CDK6 overexpressing CDXs
203 (Supplementary Fig. 9A-D). To assess whether a reduction in DNA replication stress and genomic
204 instability also accompanied these effects, we assessed Ki-67, p-Rb, p-RPA, and γ-H2AX

205 expression in tumors treated with either osimertinib or palbociclib alone or in combination.
206 Osimertinib plus palbociclib-treated tumors exhibited decreased Ki-67 expression (Fig. 4A, B), as
207 well as reduced expression of p-Rb, p-RPA, and γ-H2AX compared to tumors treated with either
208 drug alone (Fig. 4C-F). Osimertinib plus palbociclib-treated tumors also exhibited increased
209 apoptosis, demonstrated by increased expression of cleaved caspase 3 (Supplementary Fig. 9E, F).
210 The percentage of CDK4-positive cells was also decreased in osimertinib plus palbociclib-treated
211 tumors (Fig. 4G, H), suggesting that CDK4/6 inhibition may lead to the elimination of cells with
212 CDK4 upregulation and concomitant CDK4-induced DNA replication stress and genomic
213 instability. Overall, these findings demonstrate that combined EGFR and CDK4/6 inhibition
214 reduces proliferation, DNA replication stress, and genomic instability associated with CDK4 or
215 CDK6 upregulation, resulting in increased tumor cell apoptosis and tumor regression.

216 We extended these findings to primary EGFR-mutant PDX (Supplementary Fig. 1) and
217 PDO (Supplementary Fig. 3) models harboring concurrent *CDK6* amplification or overexpression.
218 We included abemaciclib, another CDK4/6 inhibitor, to verify that the observed effects are
219 consistent across different CDK4/6 inhibitors. In line with the CDK4-overexpressing CDX data,
220 we found that combination treatment with osimertinib and abemaciclib was sufficient to induce
221 regression of CDK6 overexpressing primary EGFR-mutant PDOs (Supplementary Fig. 10A). To
222 investigate whether *CDK6* amplification induces DNA replication stress and genomic instability
223 that can be overcome by CDK4/6 inhibition in a more clinically relevant model, we utilized a PDX
224 model (TH116) developed from a LUAD patient biopsy at resistance to osimertinib treatment,
225 which harbored concurrent *EGFR* p.L858R mutation and *CDK6* amplification (Supplementary
226 Fig. 1E, F, and Supplementary Tables 1-2). EGFR-mutant, *CDK6*amp TH116 PDXs demonstrated
227 continued growth during osimertinib treatment, indicating EGFR TKI resistance (Supplementary

228 Fig. 10B, C). Similar to CDK6 overexpressing CDX models, these *CDK6*amp, EGFR-mutant
229 PDXs maintained high p-Rb phosphorylation when treated with osimertinib at doses sufficient to
230 suppress EGFR and ERK phosphorylation (Fig. 5A). The PDXs also demonstrated high levels of
231 the DNA replication stress and DNA damage markers TPX2, p-AURKA, in the osimertinib-treated
232 tumors (Fig. 5A). γ-H2AX was also elevated in vehicle and osimertinib-treated tumors, consistent
233 with DNA damage (Fig. 5B, C). An enrichment of CDK6-positive nuclei was observed upon
234 osimertinib treatment, suggesting that EGFR inhibition may lead to the selection of cells with
235 upregulated nuclear CDK6 (Fig. 5B, D, E). Treatment of TH116 PDXs with palbociclib, either
236 alone or in combination with osimertinib, significantly reduced both γH2AX levels as well as FGA
237 (Fig. 5C, F) and decreased tumor growth more than osimertinib alone (Supplementary Fig. 10C-
238 F). The combinatorial treatment of osimertinib with palbociclib resulted in the highest degree of
239 FGA reduction, although not statistically significant compared to monotherapy with osimertinib
240 (Fig. 5F). Mutant Allele Frequency (MAF) and TMB were also assessed to evaluate overall
241 genomic burden, but neither showed significant changes across treatment groups (Supplementary
242 Fig. 10G, H).

243 Overall, these results suggest that combinatorial treatment with osimertinib and a CDK4/6
244 inhibitor in CDK4/6-upregulated and CDK6-amplified EGFR-mutant LUAD CDX and PDX
245 models is effective and significantly reduces DNA replication stress and genomic instability, as
246 evidenced by decreased expression of DNA replication stress and DNA damage markers (γ-H2AX,
247 p-RPA), reduced Ki-67 and p-Rb levels, and lower FGA.

248

249 ***CDK4* and *CDK6* copy-number alterations are associated with significantly increased**
250 **genomic instability in EGFR-mutant LUAD patient tumors.**

251 To extend our preclinical findings and assess the clinical relevance of CDK4 and CDK6
252 CNAs in EGFR-mutant LUAD, we analyzed two large clinical datasets: Foundation Medicine (n
253 = 660) and MSK-IMPACT GENIE (n = 1983), comprising a combined total of 2,643 EGFR-
254 mutant advanced LUAD cases (Supplementary Table 3). Utilizing targeted exome sequencing data
255 across 401 cancer-relevant genes, Foundation Medicine cases were stratified into two groups:
256 tumors with cell cycle gene alterations, based on TCGA definitions, and those without
257 (Supplementary Fig. 11A, B). Among cell cycle-altered tumors, frequent events included deletions
258 or mutations in tumor suppressors *CDKN2A* (49.0%), *CDKN2B* (38.7%), and *RB1* (21.8%),
259 followed by CNAs in *CDK4* (15.7%), *CCNE1* (10.1%), *CCND1* (8.1%), and *CDK6* (6.7%). *CDK4*
260 and *CDK6* alterations were significantly enriched in EGFR-mutant versus KRAS-mutant LUAD
261 (Supplementary Fig. 11C), were mutually exclusive from one another (Supplementary Fig. 11D,
262 E), and predominantly represented by copy number gains (Supplementary Fig. 11F, G) in the
263 MSK-IMPACT GENIE and Foundation Medicine clinical cohorts. To evaluate the relationship
264 between *CDK4/6* CNAs and genomic instability, we quantified the FGA and TMB as surrogate
265 markers. EGFR-mutant LUAD harboring cell cycle gene alterations exhibited significantly
266 elevated FGA and TMB relative to cell cycle-negative tumors across both datasets (Fig. 6A, B,
267 and Supplementary Fig. 12A, B). Subgroup analysis further revealed that tumors with *CDK4* or
268 *CDK6* CNAs had markedly increased FGA (Fig. 6C, D). Tumors with *CDK4* CNAs showed
269 increased FGA in the MSK-IMPACT, but not the Foundation Medicine dataset (Fig. 6E, F),
270 whereas those with *CDK6* CNAs demonstrated increased FGA in both datasets (Fig. 6G, H). FGA
271 correlated with the degree of copy number gain of *CDK4* or *CDK6* (Fig. 6I). Notably, no
272 corresponding increase in TMB was observed with *CDK4* or *CDK6* CNA, similar to our findings
273 in preclinical models (Supplementary Fig. 12C–H). *CDK6* CNAs were associated with higher

274 FGA compared to *CDK4* CNAs in the Foundation Medicine dataset (Supplementary Fig. 12I), but
275 not the MSK-IMPACT (Supplementary Fig. 12J). *RB1*-altered tumors also demonstrated an
276 increase in FGA compared to *RB1*-non-altered tumors (Fig. 6J); however the vast majority of
277 tumors with *CDK4/6* CNAs were not found to have *RB1* alterations (Fig. 6K, L). CNAs in *CCND1*,
278 *CCND3*, *CDKN2A*, *CDKN2B*, or *CCNE1* exhibited minimal impact on FGA (Supplementary Fig.
279 13A–E). Importantly, *TP53* mutations were evenly distributed between cell cycle-positive and cell
280 cycle-negative cohorts (68.3% vs. 62.7%, p = 0.13; Supplementary Fig. 11A, B), suggesting that
281 *TP53* status alone did not account for the increased FGA. To determine whether increased FGA
282 was specific to *CDK4/6*-related alterations, we evaluated tumors with *MDM2* and *NFKBIA*
283 amplifications, commonly observed in EGFR-mutant LUAD. Neither *MDM2* nor *NFKBIA*
284 amplification was associated with increased FGA (Supplementary Fig. 13F, G), highlighting the
285 specificity of *CDK4/6* amplificaton on FGA. Next, we assessed whole genome doubling (WGD)—
286 a hallmark of genomic instability—using TCGA WES data. Tumors harboring *CDK4* or *CDK6*
287 amplification demonstrated significant enrichment for WGD events (Supplementary Fig. 13H–K),
288 supporting the conclusion that *CDK4* or *CDK6* amplification contributes to genomic instability.
289

290 **Integrative single-cell and bulk RNA sequencing analyses reveal *CDK4/6* amplification–**
291 **associated transcriptional reprogramming.**

292 To determine whether the gene expression changes identified in CDK4/6-overexpressing
293 H1975 CDXs are also present in patient tumors, we analyzed bulk RNA-seq data from the OncoSG
294 EGFR-mutant LUAD cohort. *CDK4/6*-amplified (n = 9) were compared to *CDK4/6* non-amplified
295 tumors (n = 84). Patient tumors showed significantly higher expression of six genes—*AGR2*,

296 *ASNS*, *CCZ1B*, *GGCT*, *PSMA2*, and *STEAP1* that were previously found to be upregulated in the
297 CDX model (Fig. 3 and Supplementary Fig. 14). To verify these findings in an independent cohort,
298 we analyzed single-cell RNA sequencing data from a cohort of EGFR-mutant LUAD clinical
299 samples collected at our institution (35). This cohort included three tumors with *CDK4*
300 amplification and 11 tumors from patients without *CDK4* or *CDK6* amplificaiton based on clinical
301 sequencing data and confirmed by whole exome sequencing. No tumors with *CDK6* amplification
302 were identified. UMAP visualizations demonstrated higher cancer cell–specific expression of
303 *CDK4* in *CDK4* amplified tumors compared to *CDK4/6*wt tumors (Fig. 7A-D). Significantly
304 higher expression of *AGR2*, *ASNS*, *GGCT*, *STEAP1*, and *CCZ1B,* but not *PSMA2,* was also found
305 in *CDK4* amplified compared to non-amplified tumors (Fig. 7E and Supplementary Fig. 15 A, B).
306 Spearman correlation analyses revealed positive correlations between *CDK4* expression and
307 *STEAP1*, *AGR2*, and *ASNS* in cancer cells from *CDK4*-amplified tumors compared to non-
308 amplified tumors (Fig. 7F). These genes have been implicated in promoting tumor progression
309 across multiple cancer types (29-31). In addition to higher expression of these cancer-promoting
310 genes, *CDK4*amp tumors exhibited significantly higher epithelial-mesenchymal transition (EMT)
311 scores compared to non-amplified tumors (Fig. 7G). These findings suggest that *CDK4*
312 amplification may promote transcriptional programs, including EMT, associated with aggressive
313 tumor behavior.
314

315 **Discussion**

316 This study provides a mechanistic framework for how complex somatic genetic
317 interactions shape the biology and therapeutic vulnerabilities oncogene-driven lung
318 adenocarcinoma (Fig. 8). By combining genomic analyses with preclinical models and patient-

319 derived xenografts, we demonstrate that amplification of *CDK4* or *CDK6*—occurring in
320 approximately 10% of EGFR-mutated lung cancer cases—can drive DNA replication stress,
321 genomic instability, and resistance to EGFR tyrosine kinase inhibitors.

322 We show that *CDK4/6* amplification is associated with an increased fraction of genome
323 altered (FGA) in two large independent patient cohorts (Foundation Medicine and MSK-IMPACT
324 GENIE), linking copy number gains with chromosomal instability. These findings are clinically
325 significant, as increased FGA has been associated with poor prognosis and recurrence in NSCLC
326 (36). Similarly, in the TRACERx study, increased copy number heterogeneity was associated with
327 genomic instability and increased risk of recurrence or death (37,38). Interestingly, other cell cycle
328 alterations, such as *CCNE1* amplification or *CDKN2A/2B* deletions, were not associated with
329 increased FGA, underscoring the specificity of the CDK4/6 effect. Moreover, *CCNE1*
330 amplification was mutually exclusive with *CDK4/6* amplification, suggesting distinct and non-
331 redundant roles in tumor biology.

332 Mechanistically, *CDK4/6* amplification overrides the G1 arrest typically induced by EGFR
333 TKI treatment (39), enabling continued S-phase entry and proliferation. In both treatment-naïve
334 and osimertinib-treated xenografts, *CDK4/6* overexpression correlated with sustained p-Rb
335 signaling, increased EdU and Ki-67 labeling, and upregulation of DNA replication stress and DNA
336 damage response markers, including TPX2, γ-H2AX, p-RPA, and p-ATM. Upregulation of TPX2,
337 a transcriptional target of E2F (24,26), is associated with AURORA Kinase A activation and
338 EGFR inhibitor resistance (22), suggesting one potential downstream mechanism by which
339 *CDK4/6* amplification promotes EGFR TKI resistance. Similarly, activation of ATM has been
340 associated with EGFR-mutant lung cancer cell survival and EGFR TKI resistance (21). Activation

341 of TPX2-AURKA and ATM as a result of replication stress and DNA damage may thus represent
342 two mechanisms by which *CDK4/6* amplification promotes EGFR TKI resistance (Fig. 8).

343 In the context of promoting cell cycle progression, replication stress, and DNA damage,
344 CDK4 and CDK6 activation led to recurrent copy number changes of *AGR2*, *ASNS*, and *STEAP1*
345 in both preclinical models, patient-derived xenografts, and in patient tumors. Intriguingly, *ASNS*
346 and *AGR2* have been associated with WNT/β-catenin activation (29,40), while *AGR2* and *STEAP1*
347 have been associated with EMT (31,40). WNT/β-catenin and EMT have each been associated with
348 EGFR TKI resistance (10,41,42), suggesting additional mechanisms by which *CDK4/6*
349 amplification contribute to poor response to EGFR TKI treatment. Indeed, we found that *CDK4*
350 amplified EGFR-mutated lung cancer cells demonstrated increased expression of genes associated
351 with EMT compared to *CDK4* non-amplified cancer cells in single-cell RNA-sequencing analysis
352 of patient tumors. This finding resonates with recent evidence that *RB1* loss promotes reversible
353 lineage plasticity and accelerates EGFR TKI resistance by enabling resistant mesenchymal states
354 (43). Together, these observations point to a convergent role of the CDK4/6-RB axis in promoting
355 transcriptional plasticity and EMT, highlighting that therapeutic resistance in lung cancer may be
356 shaped as much by adaptive cell-state transitions as by proliferative signaling.

357 To overcome the pro-tumor effects of *CDK4/6* amplification we explored combinatorial
358 therapy targeting EGFR and CDK4/6. Combined osimertinib and CDK4/6 inhibitor reatment
359 suppressed proliferation, reduced DNA damage and chromosomal alterations, and induced
360 apoptosis in EGFR-mutant tumors with *CDK4* or *CDK6* amplification or overexpression. This
361 highlights a potential therapeutic strategy for delaying or preventing resistance, which should be
362 further evaluated in clinical trials in biomarker-selected patients. A phase II trial of osimertinib
363 and the CDK4/6 inhibitor abemaciclib has been completed; however, results are not yet publicly

364 available. This trial was open to patients regardless of *CDK4/6* amplification status. Based on our
365 data, we predict that biomarker selection for patients with *CDK4/6* amplification will be necessary
366 to observe meaningful clinical benefit.

367 Our study has limitations. We focused primarily on canonical cell cycle functions of
368 CDK4/6, while emerging roles in immune modulation, metabolism, and transcriptional regulation
369 remain unexplored in this context (44). Here, we also highlight a link to EMT programs in single-
370 cell analyses, where only *CDK4*-amplified tumors were available, suggesting that *CDK4*
371 amplification may promote resistance through transcriptional reprogramming toward
372 mesenchymal phenotypes. Further analyses will be needed to determine whether *CDK6*
373 amplification has a similar effect. Additionally, sequencing approaches limited the detection of
374 low-frequency subclones and non-coding regulatory alterations that may contribute to resistance
375 evolution. Future studies will be needed to address these dimensions across broader cohorts.

376 In summary, we uncovered multiple mechanisms of EGFR inhibitor resistance in LUAD
377 driven by CDK4/6 hyperactivation. CDK4/6 hyperactivation promotes continued cell proliferation
378 during EGFR TKI treatment, which leads to DNA replication stress and DNA damage, resulting
379 in TPX2 and ATM activation, known drivers of EGFR TKI resistance. DNA replication stress and
380 damage in turn lead to chromosomal instability with increased copy-number changes, which
381 include copy-number gains in genes associated with EMT-associated transcriptional plasticity
382 (Fig. 8). These findings establish a rationale for therapeutic strategies combining EGFR and
383 CDK4/6 inhibitors to suppress primary oncogenic signaling and prevent replication stress and
384 DNA damage and their downstream consequences. This also has potential therapeutic implications
385 for other cancers that harbor co-activation of oncogenes within the RTK-RAS-MAPK pathway
386 concurrent with cell cycle promoting genomic alterations, which occur in a high proportion of

387 epithelial malignancies. More broadly, our work illustrates how co-occurring genomic alterations
388 and transcriptional programs synergistically shape tumor evolution and therapy response.
389
390 **Methods**
391 **Cell Lines, Primary Organoids and Reagents**
392 All cell lines were obtained and cultured according to the American Type Culture Collection
393 (ATCC) recommendations. Before testing, cell lines were authenticated through STR profiling and
394 confirmed negative for mycoplasma contamination. EGFR mutant (EGFRmt) LUAD cell lines
395 used in the present study were H1975 (EGFR L858R, T790M), HCC827 (EGFR Del19), and PC9
396 (EGFR Del19). EGFR-mutant cells were cultured in RPMI 1640 medium (HyClone, GE
397 Healthcare), containing 10% FBS (SAFC, Sigma-Aldrich) and 1X penicillin and streptomycin
398 (HyClone, GE Healthcare). DMEM (HyClone, GE Healthcare) supplemented with 10% FBS, 0.1X
399 penicillin, and streptomycin was used for HEK293-FT cells. All cell lines were cultured in a
400 humidified incubator with 5% CO_2 at 37 °C. Primary, patient-derived organoid TH-107 cells were
401 established from a biopsy specimen and cultured in Matrigel as described previously(45,46). Drugs
402 used in these studies were Osimertinib, Abemaciclib (Selleckchem), and Palbociclib (LC
403 Laboratories). The antibodies used for immunoblotting, immunohistochemistry, and
404 immunofluorescence were: CDK4 (Cell Signaling Tech., 12790) CDK6 (Cell Signaling Tech.,
405 3136), pEGFR-Tyr1086 (ThermoFisher, 369700), p-EGFR-Tyr1068 (Cell Signaling Tech., 3777),
406 EGFR L858R (Cell Signaling Tech., 3197), p-AURKA (Cell Signaling Tech., 3079), p-Akt (Cell
407 Signaling Tech., 4060), p-ERK (Cell Signaling Tech., 4370), Actin (Sigma, A2228), Rb (Cell
408 Signaling Tech., 9309), p-Rb-Ser780 (Cell Signaling Tech., 9307), p-Rb-Ser807/811 (Cell
409 Signaling Tech., 8516), CCNE1 (Cell Signaling Tech., 20808), TPX2 (Cell Signaling Tech.,

410 12245), cleaved caspase 3 (Cell Signaling Tech., 9661), p-RPA (Bethyl Laboratories, A300 245A
411 M), p-ATM (Cell Signaling Tech., 13050), RPA (Bethyl Laboratories, A300 244A), γ-H2AX
412 (EMD Millipore, 05-636), ki67 (Leica, NCL-L-Ki67-MM1). All antibodies were diluted per the
413 datasheet recommendations. Small interfering RNAs for E2F1 and scramble control were
414 purchased from Dharmacon, and transient knockdown was induced following the manufacturer's
415 instructions.
416
417 **Lentiviral Infection, Soft Agar, and Crystal Violet Assays**
418 Mammalian expression vectors EGFP, CDK4, and CDK6 were purchased from Origene.
419 Knockdown lentiviral constructs for CDK4 and a scramble plasmid were purchased from SIGMA.
420 Transfection of HEK293-FT cells with the overexpressing vectors was performed using Mirus
421 reagent, per the manufacturer's instructions. Viral particles were collected after 72 hrs of
422 transfection to infect EGFR-mutant LUAD cells in a medium containing polybrene (8 μg/ml;
423 Sigma-Aldrich). After 72 hrs, cells were sorted for EGFP or selected with puromycin (1 μg/mL;
424 Gibco). Selected cells were used in the in vitro and in vivo tests. Successful overexpression of
425 CDK4 and CDK6 was confirmed by qPCR and/or immunoblotting.
426 In vitro, soft-agar colony formation assay was performed as previously described(47). Colonies'
427 growth was assessed for up to 4 weeks in the presence of osimertinib (10-100 nM) or DMSO
428 control. At the time of collection, 6-well soft agar plates were incubated with a solution of 0.005%
429 crystal violet in water for three hours. Plates were then imaged using ImageQuant (GE Healthcare),
430 and colonies were counted using the ImageJ program (NIH).
431
432 **Preclinical Studies**

433 H1975, PC9 xenografts, and TH-116 PDXs were established in compliance with the UCSF IACUC
434 IRB-approved protocols. Each H1975 and PC9 flank xenograft was obtained after subcutaneous
435 injection of 1 million cells in each 4-week-old female SCID or athymic mouse flank. NSG mice
436 were used for the propagation and establishment of TH-116 PDXs. Osimertinib was reconstituted
437 for in vivo experiments following previously published work (48). Osimertinib treatments were
438 performed by daily oral gavage (dose range assessed: 2.5 mg/Kg, 5 mg/Kg, 10 mg/Kg). Mice
439 euthanasia was done when xenografts reached 20 mm in diameter. We used similar drug regimens
440 for combination studies. Mice were randomly divided and kept unlabeled until the treatments
441 started. Multiple researchers measured the tumors with a digitized caliper.
442 IP injections of 100 μL EdU (200 μg) solution in PBS were carried out 48 hrs before xenografts
443 resection (Click-iT EdU kit, Invitrogen)(49) to assess the degree of newly synthesized DNA. OCT
444 blocks of tissues were collected from each tumor and used for deriving cryosections that were
445 stained either following the manufacturer's protocol for single EdU stain (Click-iT EdU kit,
446 Invitrogen) or double immunofluorescence stain with γH2AX (50).
447
448 **Immunoblotting, Immunohistochemistry, Immunofluorescence**
449 Protein lysates were extracted in RIPA buffer, adding protease inhibitors (Roche) and phosphatase
450 inhibitors (Roche). For the immunoblotting, 15 μg of proteins were loaded into precast 4–15%
451 acrylamide gels (Bio-Rad), then transferred to nitrocellulose membranes with the Trans-blot Turbo
452 Transfer system (Bio-Rad). Blots were blocked for 1 hr at room temperature in Tris-buffered
453 saline, 0.1% Tween20 (vol/vol), and 5% (vol/vol) BSA (Fisher Scientific). Incubation with the
454 primary antibodies was performed overnight at 4 °C, after which the membranes were washed
455 twice with Tris-buffered saline, Tween20 (0.1% vol/vol). Incubation with secondary HRP-

456 conjugated antibodies (Cell Signaling Technology, anti-rabbit IgG, no. 7074, anti-mouse IgG, no.
457 7076) was run for 1 hr at room temperature. Membranes were then incubated with ECL reagent
458 (GE Healthcare), and the signal was detected by chemiluminescence. The development and
459 scanning of the blots were run with ImageQuant LAS4000 (GE Healthcare Life Sciences). ImageJ
460 (NIH) allowed western blot quantification.
461 Formalin-Fixed, Paraffin-Embedded tissue blocks and sections were provided by the UCSF
462 histology core. Immunohistochemistry (IHC) was performed as previously described (10). The
463 stained slides were scanned with Aperio ScanScope CS Slide Scanner (Aperio Technologies) using
464 a 20x objective. ScanScope algorithm was applied for the IHC quantification, considering 3-5
465 fields per section and calculating mean, and S.E.M. CDK4, CDK6, p-Rb, γ-H2AX, p-RPA stains
466 were quantified on the same areas of adjacent xenograft, viable tissue sections.
467 FFPE sections were stained with hematoxylin-eosin for the tissue necrotic area analysis, and
468 necrosis was quantified as the percentage of affected areas following pathological guidelines (51).
469

470 **Bioinformatics Analysis of CDK4/6-Overexpressing H1975 Xenografts**

471 **Fraction of Genome Alteration Analysis (FGA), SNVs, and copy number calling from whole**
472 **exome sequencing data from in vivo tumor tissues**

473 DNA was extracted from xenograft tissues using a tissue-DNA extraction-specific kit (Qiagen)
474 and sent to Novogene (Sacramento, USA) for whole exome sequencing (WES; NovaSeq 6000,
475 PE150, 200X). Pair-end .fastq files were mapped to the hg19 genome. Mutation (SNVs) calling
476 was done using the SeqMule pipeline. The .vcf files were annotated using ANNOVAR software
477 at a high-performance computing cluster (UCSF Helen Diller Comprehensive Cancer Center).
478 Further analysis of annotated variants was conducted under the RStudio/R environment. Cell-

479 derived and patient-derived xenograft WES bam files were used to infer copy number alterations
480 between the treatment and control groups, utilizing the "copy number" function in the VarScan
481 algorithm. The altered genomic segments were annotated at the gene level. Each gene length was
482 retrieved from hsapiens.UCSC.hg19.knownGene database. The sum of altered CNV genes over
483 the size of captured WES was defined as a Fraction of Genome Alterations (FGA). We normalized
484 the CDK4/6 overexpressing and CDK6 amp xenografts FGA with the FGA from empty vector,
485 CDK4/6 wild type, or vehicle-treated control xenografts expressing it as a fold-change (52). To
486 infer the absolute integer gene copy number, mapped BAM files were used as input along with
487 hg19_SureSelect_Human_All_Exon_V5.bed and human_g1k_v37.fasta files for CNVkit (default
488 parameters, python library, https://cnvkit.readthedocs.io/en/stable/), and the log2 ratio of estimated
489 segmentation between two conditions was computed to identify regions significantly affected by
490 CNVs.

491 **RNA sequencing and GSEA**

492 Total RNAs were extracted from CDK4/6 overexpressing tissues and empty vector controls
493 (Qiagen) and sent to Novogene for RNA sequencing (NovaSeq 6000, PE150).
494 For the Gene Set Enrichment Analysis (GSEA), a gene expression matrix for CDK4 and CDK6
495 overexpressing tissues, and controls (cells expressing empty vector, E.V.) in triplicate was
496 imported into the GSEA algorithm (v4.03, Broad Institute). MSigDB was used for gene set
497 enrichment comparisons between CDK4/6 overexpressing and E.V. CDXs groups. The
498 enrichment score (ES), normalized ES, and False discovery rate (FDR) were provided by the
499 algorithm. An FDR < 25% was used for exploratory enrichment analysis.

500 **Integration of Gene Expression and Copy Number**

501 Differential Gene Expression Analysis (Vehicle Group) RNA-seq differential expression results
502 were obtained from CDK4-, CDK6-, and EGFP (E.V.)-overexpressing H1975-derived xenografts
503 in the vehicle-treated group. Gene-level $\log_2$ fold changes and FDR-adjusted p-values were
504 provided for CDK4 vs. EGFP and CDK6 vs. E.V. comparisons. Differentially expressed (DE)
505 genes were identified using relaxed criteria: $|\log_2 \text{ fold change}| \geq 0.3$ and false discovery rate (FDR)
506 ≤ 0.3. Volcano plots were generated to visualize differential gene expression. Genes were color-
507 coded based on significance and direction of change: upregulated (red), downregulated (blue), or
508 not significant (grey). Selected genes of interest (e.g., AGR2, CBX3, ANLN) were annotated for
509 interpretability. DE analyses were conducted before and after Xengsort filtering, which removed
510 approximately 6% mouse reads to assess potential bias from murine stromal contamination.
511 Agreement between filtered and unfiltered data was quantified using: • Pearson and Spearman
512 correlation of $\log_2$ fold change values • Fisher's exact test for overlap significance • Jaccard index
513 for DEG set similarity. These comparisons were implemented in Python v3.10 using matplotlib,
514 seaborn, and matplotlib-venn. Results demonstrated near-perfect consistency (e.g., CDK4 DE:
515 Pearson r = 1.000, Jaccard = 0.991), confirming minimal impact of mouse filtering on DE calls.
516 Copy number variants (CNVs) were inferred from whole-exome sequencing (WES) data using
517 CNVkit, with normalization performed relative to the EGFP (E.V.) control group. CNVkit-derived
518 results were summarized as $\log_2$-transformed copy number ratios and estimated absolute copy
519 number values per gene. Log_2 ratios reflect relative copy number changes, while absolute CN
520 values were inferred and rounded by CNVkit for discrete copy number calling. Gene CNA lists
521 were derived from the CDK4 and CDK6 upregulated CDXs by annotating the genes in the
522 chromosomal segments affected by CNAs (UCSC Genome Browser).

523 Venn diagrams were constructed to identify genes concurrently upregulated at both transcript and
524 copy number levels to visualize overlap between DE genes (RNA-seq) and CN-amplified genes
525 (CNVkit) in the vehicle-treated group.
526 Pathway Enrichment Analysis Genes overlapping between transcriptomic (vehicle group) and
527 copy number (vehicle group) datasets were converted to Entrez IDs using the bitr() function from
528 the clusterProfiler package (with org.Hs.eg.db as the reference). Functional enrichment was
529 performed via: • Gene Ontology (GO): enrichGO • KEGG pathways: enrichKEGG • Reactome
530 pathways: enrichPathway from ReactomePA. All enrichment results were adjusted using the
531 Benjamini-Hochberg FDR correction, with significance defined as adjusted $p < 0.05$. Results were
532 visualized using barplots, dotplots, and enrichment maps.
533 **Foundation Medicine, MSK-IMPACT GENIE Clinical Dataset Analyses**
534 EGFR-mutant advanced-stage LUAD cases analyzed from Foundation Medicine (FM) were 660,
535 and targeted exome sequencing data for a panel of 401 cancer-related genes were used to detect
536 somatic mutations and copy number alterations. Foundation Medicine provided the annotated data
537 matrix. FGA analysis was computed from the Foundation Medicine dataset using a panel of 306
538 cancer-related genes with CNA (gains and deletions), following previously published methods
539 (52). Briefly, patients were stratified based on the presence of selected cell cycle gene copy number
540 alterations (53). For each patient, genes with copy number alterations annotated from Foundation
541 Medicine were filtered in, and the size of each gene was retrieved. The sum of altered gene sizes
542 over the captured genome was computed as FGA. Boxplots were created with interquartile range
543 (lower quartile 25%, median, and upper quartile 75%). Each dot represents the FGA value in each
544 patient's tumor. Statistical significance was assessed using the Wilcoxon test. For the Tumor
545 Mutation Burden (TMB) analysis, the total nonsynonymous mutations over the captured genome

546 size were computed as tumor mutation burden (TMB, number of gene mutations/Mega-base).
547 Cases with concurrent *EGFR* and *CDK4/6* alterations were further analyzed for *RB1* and *TP53*
548 alteration frequencies.
549 FGA analysis was computed from the MSK-IMPACT GENIE dataset using 1983 EGFR-mutant
550 LUAD cases stratified based on the presence of selected cell cycle gene copy number alterations
551 (53) as previously described (AACR project GENIE Consortium, GENIE Cohort version 15.1 –
552 public). Cases with concurrent *EGFR* and *CDK4/6* alterations were further analyzed for *RB1* and
553 *TP53* alteration frequencies.
554 For the correlation analysis between FGA and *CDK4/6* amplifications, patients harboring
555 *CDK4/CDK6* amplifications with copy numbers greater than 4 were selected, and the value of
556 log10(CNV CDK4/6 amp) versus FGA value was plotted with a linear regression model for the
557 best-fit line, and the F-statistic was used to calculate the p-value.
558 Oncoprint analysis was used to show the most frequent concurrent gene alterations in cell cycle
559 (CC) alteration-positive (n=357) or cell cycle-alteration-negative (n=303) Foundation Medicine
560 dataset cohorts. Each column represents a patient; each row represents one gene. Gene alteration
561 frequencies greater than 6% were shown in the oncoprints.
562 Analysis of LUAD cases through cBioPortal was done by selecting cases positive for CDK4/6
563 CNAs with concurrent EGFR mutations (125 total cases).
564
565 **Whole Genome Doubling (WGD) analysis in the TCGA LUAD dataset**
566 Whole Genome Doubling (WGD) analysis from the TCGA lung adenocarcinoma (LUAD) cohort
567 dataset was downloaded from:

568 https://github.com/judithabk6/ITH_TCGA/blob/master/external_data/TCGA_mastercalls.abs_tab
569 les_JSedit.fixed.txt
570 Correlation analysis was run to annotate WGD events along with the status of *CDK4/6* amp using
571 the TCGA CNA file annotations. Fisher's exact test was used to measure the statistical
572 significance.
573
574 **Gene Expression and Statistical Analysis in OncoSG EGFR mutant Cohort**
575 Z-score normalized gene expression data were analyzed for EGFR-mutant LUAD cases in the
576 OncoSG cohort. CDK4/6-positive (n = 9) and CDK4/6-negative (n = 84) groups were compared
577 using Welch's two-sample t-test. Significance thresholds were set at $P < 0.05$. Violin plots were
578 generated in *ggplot2*, including median/interquartile boxplots and jittered sample points.
579
580 **Single-Cell RNA-seq Analysis of EGFR-Mutant UCSF Cohort**
581 Single-cell RNA-seq data from the internal UCSF EGFR-mutant cohort were processed using
582 Python (v3.8+) and Scanpy. Cells were stratified by patient group: *CDK4*amp (n = 3) vs.
583 *CDK4/6*wt (n = 11) cases. Cells annotated as cancer via inferCNV-based labeling were retained
584 for downstream analyses. UMAP coordinates were generated using single cells from *CDK4*amp
585 cases using a reproducible pipeline implemented in Python: normalization (sc.pp.normalize_total),
586 log-transformation, PCA, neighborhood graph construction, and UMAP embedding.
587 Expression of genes of interest (GOI: *AGR2*, *ASNS*, *CCZ1B*, *CDK4*, *GGCT*, *PSMA2*, and *STEAP1*)
588 was visualized on UMAPs using scaled expression values.
589 Log-normalized expression of GOIs in cancer cells was compared between *CDK4*amp and
590 *CDK4/6*wt groups. Violin and strip plots were generated using Seaborn in Python. Medians and

interquartile ranges were annotated. Between-group comparisons were assessed using Mann–Whitney U tests.

For each group, Spearman correlation coefficients (ρ) between *CDK4* and other GOIs were calculated using Python's SciPy library. Significance (two-sided) was evaluated with Spearman's rank test, with multiple testing correction via Benjamini–Hochberg FDR. Correlations (ρ) and $-\log_{10}$(p-values) were visualized as bar plots.

An EMT score was computed per cell as the mean expression of canonical EMT markers (*VIM*, *ZEB1*, *SNAI1*, *TWIST1*, *CDH2*, *FN1*). Correlations between EMT score and mean GOI expression were analyzed and visualized by group using violin and scatter plots with regression fits generated in Python. Group-specific Spearman ρ and p-values were annotated to assess differential EMT–GOI associations.

Scatter plots were generated for each GOI to assess EMT score correlations separately in *CDK4*amp and *CDK4/6*wt cancer cells. Each plot displays the Spearman ρ and p-value to illustrate gene-specific EMT associations across patient groups.

Statistical analyses

We used One-way ANOVA with Tukey's multiple comparisons and Student's T-test to assess statistical significance in preclinical functional studies (GraphPad Prism); variations across samples were expressed as S.E.M. For the Fraction of Genome Alterations (FGA) and Tumor Mutational Burden (TMB) analyses, the Wilcoxon non-parametric two-group comparison test and two-sided Student t-test assessed statistical significance. Statistics were computed using Fisher's exact test for the mutual exclusivity and WGD analyses. For the pathway enrichment analysis of SNVs, statistics were calculated using a hypergeometric test (phyper in R).

614 **Data Repositories**

615 DNA sequencing datasets included in the manuscript are available at the NCBI SRA reference
616 accession code PRJNA1093094 (release date April 28th, 2025). RNA sequencing datasets in the
617 manuscript are available at the NCBI GEO reference accession code: GSE262270 (release date
618 TBD).

619 **Acknowledgments:** This project was supported by the NIH/NCI U54CA224081 (T.G.B), The
620 Damon Runyon Cancer Research Foundation P0528804 (United States), Doris Duke Charitable
621 Foundation P2018110 (United States), V. Foundation P0530519 (to C.M.B.). The authors thank
622 Thomas B.K. Watkins for critical advice in the whole genome doubling analysis, Foundation
623 Medicine Inc. (Cambridge, Massachusetts) for supporting genomic data, Kari Herrington from the
624 UCSF Microscopy Core for the helpful advice with the immunofluorescence experiments, Robin
625 Lea for the helpful advice with the clinical dataset analyses. We gratefully acknowledge the use of
626 data from the MSK-IMPACT GENIE BioPortal, which provided valuable genomic datasets
627 essential for this study.

628
629
630
631
632
633
634
635
636
637
638
639
640
641
642
643 **References**
644

645 1. Tan AC, Tan DSW. Targeted Therapies for Lung Cancer Patients With Oncogenic Driver
646 Molecular Alterations. J Clin Oncol **2022**;40:611-25
647 2. Lynch TJ, Bell DW, Sordella R, Gurubhagavatula S, Okimoto RA, Brannigan BW*, et al.*
648 Activating mutations in the epidermal growth factor receptor underlying responsiveness
649 of non-small-cell lung cancer to gefitinib. N Engl J Med **2004**;350:2129-39
650 3. Paez JG, Jänne PA, Lee JC, Tracy S, Greulich H, Gabriel S*, et al.* EGFR mutations in lung
651 cancer: correlation with clinical response to gefitinib therapy. Science **2004**;304:1497-
652 500
653 4. Pao W, Miller VA, Politi KA, Riely GJ, Somwar R, Zakowski MF*, et al.* Acquired resistance
654 of lung adenocarcinomas to gefitinib or erlotinib is associated with a second mutation in
655 the EGFR kinase domain. PLoS Med **2005**;2:e73
656 5. Ramalingam SS, Vansteenkiste J, Planchard D, Cho BC, Gray JE, Ohe Y*, et al.* Overall
657 Survival with Osimertinib in Untreated,. N Engl J Med **2020**;382:41-50
658 6. Soria JC, Ohe Y, Vansteenkiste J, Reungwetwattana T, Chewaskulyong B, Lee KH*, et al.*
659 Osimertinib in Untreated EGFR-Mutated Advanced Non-Small-Cell Lung Cancer. N Engl J
660 Med **2018**;378:113-25
661 7. Thress KS, Paweletz CP, Felip E, Cho BC, Stetson D, Dougherty B*, et al.* Acquired EGFR
662 C797S mutation mediates resistance to AZD9291 in non-small cell lung cancer harboring
663 EGFR T790M. Nat Med **2015**;21:560-2
664 8. Lu S, Ramalingam SS. Osimertinib after Chemoradiotherapy in Stage III EGFR-Mutated
665 NSCLC. Reply. N Engl J Med **2024**;391:1555-6
666 9. Gini B, Thomas N, Blakely CM. Impact of concurrent genomic alterations in epidermal
667 growth factor receptor (J Thorac Dis **2020**;12:2883-95
668 10. Blakely CM, Watkins TBK, Wu W, Gini B, Chabon JJ, McCoach CE*, et al.* Evolution and
669 clinical impact of co-occurring genetic alterations in advanced-stage EGFR-mutant lung
670 cancers. Nat Genet **2017**;49:1693-704
671 11. Liu M, Xu S, Wang Y, Li Y, Zhang H, Liu H*, et al.* PD 0332991, a selective cyclin D kinase
672 4/6 inhibitor, sensitizes lung cancer cells to treatment with epidermal growth factor
673 receptor tyrosine kinase inhibitors. Oncotarget **2016**;7:84951-64
674 12. Sitthideatphaiboon P, Teerapakpinyo C, Korphaisarn K, Leelayuwatanakul N,
675 Pornpatrananrak N, Poungvarin N*, et al.* Co-occurrence CDK4/6 amplification serves as
676 biomarkers of de novo EGFR TKI resistance in sensitizing EGFR mutation non-small cell
677 lung cancer. Sci Rep **2022**;12:2167
678 13. Hara N, Ichihara E, Kano H, Ando C, Morita A, Nishi T*, et al.* CDK4/6 signaling attenuates
679 the effect of epidermal growth factor receptor (EGFR) tyrosine kinase inhibitors in.
680 Transl Lung Cancer Res **2023**;12:2098-112
681 14. La Monica S, Fumarola C, Cretella D, Bonelli M, Minari R, Cavazzoni A*, et al.* Efficacy of
682 the CDK4/6 Dual Inhibitor Abemaciclib in EGFR-Mutated NSCLC Cell Lines with Different
683 Resistance Mechanisms to Osimertinib. Cancers (Basel) **2020**;13
684 15. Qin Q, Li X, Liang X, Zeng L, Wang J, Sun L*, et al.* CDK4/6 inhibitor palbociclib overcomes
685 acquired resistance to third-generation EGFR inhibitor osimertinib in non-small cell lung
686 cancer (NSCLC). Thorac Cancer **2020**;11:2389-97

687 16. de Jager VD, Stigt JA, Niemantsverdriet M, Ter Elst A, van der Wekken AJ. Osimertinib
688 and palbociclib in an EGFR-mutated NSCLC with primary CDK4 amplification after
689 progression under osimertinib. NPJ Precis Oncol **2024**;8:113
690 17. Ekholm SV, Reed SI. Regulation of G(1) cyclin-dependent kinases in the mammalian cell
691 cycle. Curr Opin Cell Biol **2000**;12:676-84
692 18. Zhang C-Z, Pellman D. Cancer Genomic Rearrangements and Copy Number Alterations
693 from Errors in Cell Division. Volume 6: Annual Review of Cancer Biology; 2022. p 245-68.
694 19. Abbas T, Keaton MA, Dutta A. Genomic instability in cancer. Cold Spring Harb Perspect
695 Biol **2013**;5:a012914
696 20. Panagopoulos A, Altmeyer M. The Hammer and the Dance of Cell Cycle Control. Trends
697 Biochem Sci **2021**;46:301-14
698 21. Ali M, Lu M, Ang HX, Soderquist RS, Eyler CE, Hutchinson HM*, et al.* Small-molecule
699 targeted therapies induce dependence on DNA double-strand break repair in residual
700 tumor cells. Sci Transl Med **2022**;14:eabc7480
701 22. Shah KN, Bhatt R, Rotow J, Rohrberg J, Olivas V, Wang VE*, et al.* Aurora kinase A drives
702 the evolution of resistance to third-generation EGFR inhibitors in lung cancer. Nat Med
703 **2019**;25:111-8
704 23. Haderk F, Chou YT, Cech L, Fernández-Méndez C, Yu J, Olivas V*, et al.* Focal adhesion
705 kinase-YAP signaling axis drives drug-tolerant persister cells and residual disease in lung
706 cancer. Nat Commun **2024**;15:3741
707 24. Wu L, Timmers C, Maiti B, Saavedra HI, Sang L, Chong GT*, et al.* The E2F1-3 transcription
708 factors are essential for cellular proliferation. Nature **2001**;414:457-62
709 25. Ren L, Chen L, Wu W, Garribba L, Tian H, Liu Z*, et al.* Potential biomarkers of DNA
710 replication stress in cancer. Oncotarget **2017**;8:36996-7008
711 26. Byrum AK, Carvajal-Maldonado D, Mudge MC, Valle-Garcia D, Majid MC, Patel R*, et al.*
712 Mitotic regulators TPX2 and Aurora A protect DNA forks during replication stress by
713 counteracting 53BP1 function. J Cell Biol **2019**;218:422-32
714 27. Dasika GK, Lin SC, Zhao S, Sung P, Tomkinson A, Lee EY. DNA damage-induced cell cycle
715 checkpoints and DNA strand break repair in development and tumorigenesis. Oncogene
716 **1999**;18:7883-99
717 28. Lachmann A, Xu H, Krishnan J, Berger SI, Mazloom AR, Ma'ayan A. ChEA: transcription
718 factor regulation inferred from integrating genome-wide ChIP-X experiments.
719 Bioinformatics **2010**;26:2438-44
720 29. Cai DJ, Zhang ZY, Bu Y, Li L, Deng YZ, Sun LQ*, et al.* Asparagine synthetase regulates lung-
721 cancer metastasis by stabilizing the β-catenin complex and modulating mitochondrial
722 response. Cell Death Dis **2022**;13:566
723 30. Fessart D, Domblides C, Avril T, Eriksson LA, Begueret H, Pineau R*, et al.* Secretion of
724 protein disulphide isomerase AGR2 confers tumorigenic properties. Elife **2016**;5
725 31. Huo SF, Shang WL, Yu M, Ren XP, Wen HX, Chai CY*, et al.* STEAP1 facilitates metastasis
726 and epithelial-mesenchymal transition of lung adenocarcinoma via the JAK2/STAT3
727 signaling pathway. Biosci Rep **2020**;40

728 32. Lin Z, Xiong L, Zhou J, Wang J, Li Z, Hu H*, et al.* γ-Glutamylcyclotransferase Knockdown
729 Inhibits Growth of Lung Cancer Cells Through G0/G1 Phase Arrest. Cancer Biother
730 Radiopharm **2015**;30:211-6
731 33. Bosso G, Cipressa F, Tullo L, Cenci G. Co-amplification of CBX3 with EGFR or RAC1 in
732 human cancers corroborated by a conserved genetic interaction among the genes. Cell
733 Death Discov **2023**;9:317
734 34. Suzuki C, Daigo Y, Ishikawa N, Kato T, Hayama S, Ito T*, et al.* ANLN plays a critical role in
735 human lung carcinogenesis through the activation of RHOA and by involvement in the
736 phosphoinositide 3-kinase/AKT pathway. Cancer Res **2005**;65:11314-25
737 35. Maynard A, McCoach CE, Rotow JK, Harris L, Haderk F, Kerr DL*, et al.* Therapy-Induced
738 Evolution of Human Lung Cancer Revealed by Single-Cell RNA Sequencing. Cell
739 **2020**;182:1232-51.e22
740 36. Zhou J, Sanchez-Vega F, Caso R, Tan KS, Brandt WS, Jones GD*, et al.* Analysis of Tumor
741 Genomic Pathway Alterations Using Broad-Panel Next-Generation Sequencing in
742 Surgically Resected Lung Adenocarcinoma. Clin Cancer Res **2019**;25:7475-84
743 37. Jamal-Hanjani M, Wilson GA, McGranahan N, Birkbak NJ, Watkins TBK, Veeriah S*, et al.*
744 Tracking the Evolution of Non-Small-Cell Lung Cancer. N Engl J Med **2017**;376:2109-21
745 38. Frankell AM, Dietzen M, Al Bakir M, Lim EL, Karasaki T, Ward S*, et al.* The evolution of
746 lung cancer and impact of subclonal selection in TRACERx. Nature **2023**;616:525-33
747 39. Cross DA, Ashton SE, Ghiorghiu S, Eberlein C, Nebhan CA, Spitzler PJ*, et al.* AZD9291, an
748 irreversible EGFR TKI, overcomes T790M-mediated resistance to EGFR inhibitors in lung
749 cancer. Cancer Discov **2014**;4:1046-61
750 40. Zheng C, Mao Y, Ye J, Zhang M, Chen Y. Function and mechanism of exogenous AGR2 in
751 colorectal cancer cells. Heliyon **2024**;10:e28175
752 41. Yue P, He Y, Zuo R, Gong W, Wang Y, Chen L*, et al.* CCDC34 maintains stemness
753 phenotype through β-catenin-mediated autophagy and promotes EGFR-TKI resistance in
754 lung adenocarcinoma. Cancer Gene Ther **2025**;32:104-21
755 42. Yauch RL, Januario T, Eberhard DA, Cavet G, Zhu W, Fu L*, et al.* Epithelial versus
756 mesenchymal phenotype determines in vitro sensitivity and predicts clinical activity of
757 erlotinib in lung cancer patients. Clin Cancer Res **2005**;11:8686-98
758 43. Zhang L, Chinnam M, Balk B, Zhang X, Wang Y, Shaurova T*, et al.* Reversible therapeutic
759 resistance in EGFR mutant lung cancer caused by RB1 loss
760 induced lineage plasticity. bioRxiv **2025**:2025.08.04.668485
761 44. Fassl A, Geng Y, Sicinski P. CDK4 and CDK6 kinases: From basic science to cancer
762 therapy. Science **2022**;375:eabc1495
763 45. Seino T, Kawasaki S, Shimokawa M, Tamagawa H, Toshimitsu K, Fujii M*, et al.* Human
764 Pancreatic Tumor Organoids Reveal Loss of Stem Cell Niche Factor Dependence during
765 Disease Progression. Cell Stem Cell **2018**;22:454-+
766 46. Barbosa Rabago D, Blakely CM, Haderk F, Bivona TG. Profiling Sensitivity to Targeted
767 Therapies in EGFR-Mutant NSCLC Patient-Derived Organoids. J Vis Exp **2021**
768 47. Horibata S, Vo TV, Subramanian V, Thompson PR, Coonrod SA. Utilization of the Soft
769 Agar Colony Formation Assay to Identify Inhibitors of Tumorigenicity in Breast Cancer
770 Cells. Jove-Journal of Visualized Experiments **2015**

771 48. Nanjo S, Wu W, Karachaliou N, Blakely CM, Suzuki J, Chou YT*, et al.* Deficiency of the
772 splicing factor RBM10 limits EGFR inhibitor response in EGFR-mutant lung cancer. J Clin
773 Invest **2022**;132
774 49. Salic A, Mitchison TJ. A chemical method for fast and sensitive detection of DNA
775 synthesis in vivo. Proceedings of the National Academy of Sciences of the United States
776 of America **2008**;105:2415-20
777 50. Solovjeva L, Firsanov D, Pleskach N, Svetlova M. Immunofluorescence Analysis of γ-H2AX
778 Foci in Mammalian Fibroblasts at Different Phases of the Cell Cycle. In: Didenko VV,
779 editor. Fast Detection of DNA Damage: Methods and Protocols. New York, NY: Springer
780 New York; 2017. p 187-94.
781 51. Kumar V, Abbas AK, Fausto N, Aster JC. Robbins and Cotran Pathologic Basis of Disease,
782 Professional Edition E-Book. Elsevier Health Sciences; 2014.
783 52. Zhou J, Sanchez-Vega F, Caso R, Tan KS, Brandt WS, Jones GD*, et al.* Analysis of Tumor
784 Genomic Pathway Alterations Using Broad-Panel Next-Generation Sequencing in
785 Surgically Resected Lung Adenocarcinoma. Clin Cancer Res **2019**
786 53. Sanchez-Vega F, Mina M, Armenia J, Chatila WK, Luna A, La KC*, et al.* Oncogenic
787 Signaling Pathways in The Cancer Genome Atlas. Cell **2018**;173:321-+
788
789
790
791

Figure 1

A

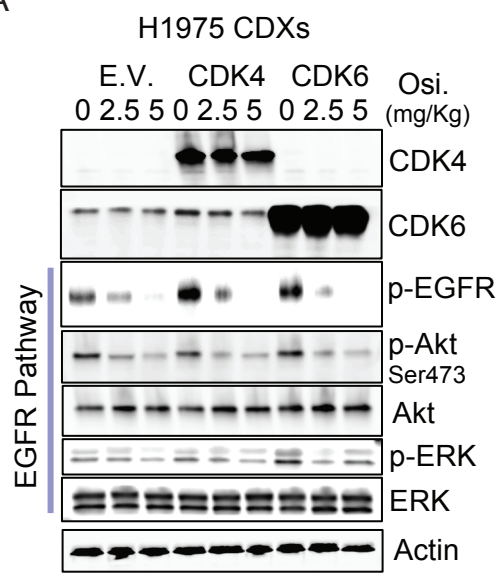

B

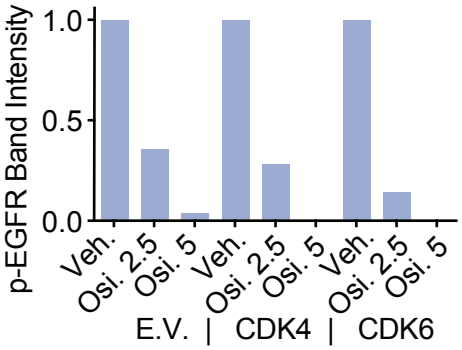

C

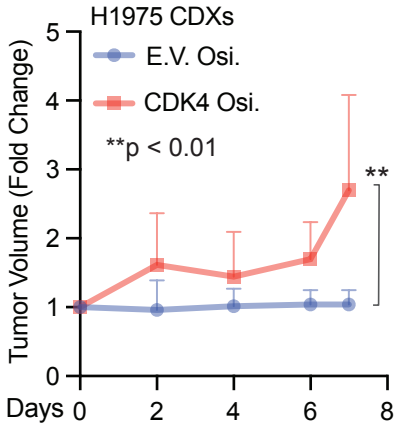

D

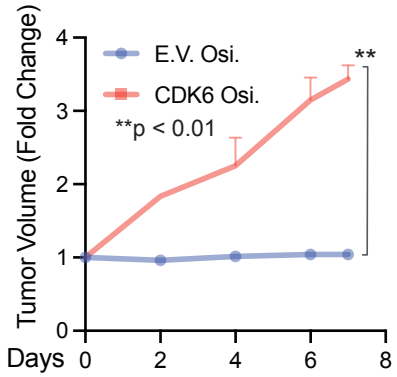

E

Pathway UP (FDR q-val. < 0.05)	CDK4 NES vs E.V.	CDK6 NES vs E.V.
E2F_TARGETS	3.0660121	3.0148368
G2M_CHECKPOINT	2.6910038	2.3356688
HALLMARK_MYC_TARGETS_V1	2.715179	1.6162359
DNA_REPAIR	1.1376647	1.5257235

F

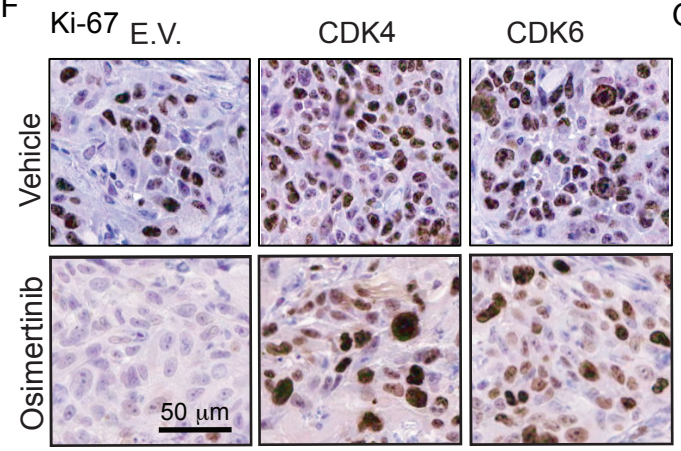

G

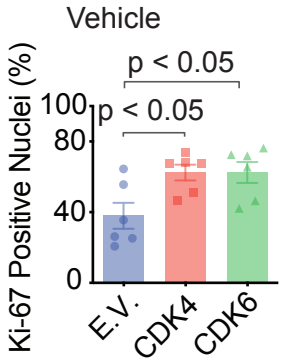

H

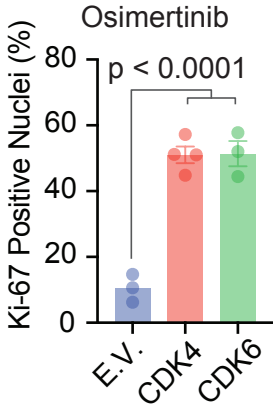

I

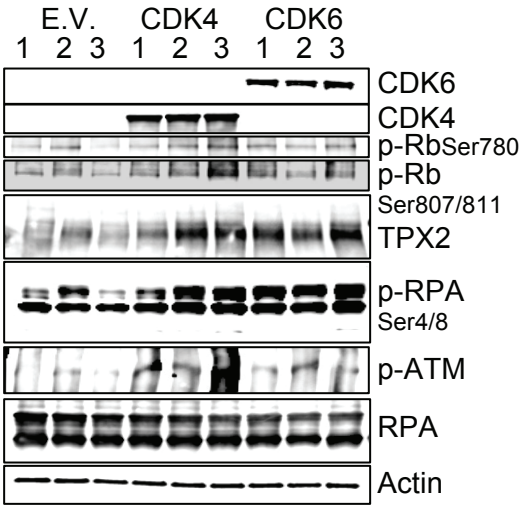

J

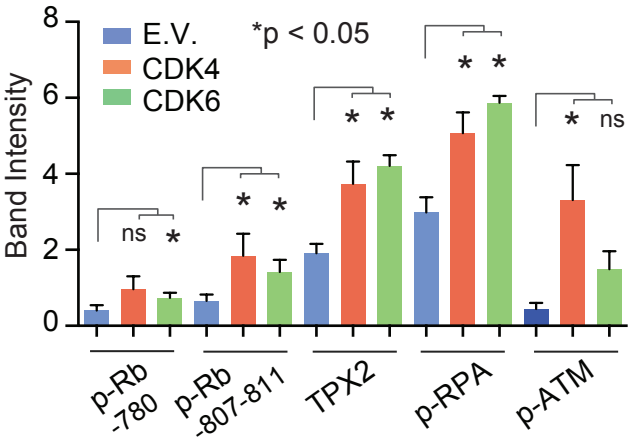

Figure 1 - CDK4/6 upregulation promotes osimertinib resistance and replication stress in EGFRmt LUAD CDXs. (A) Biochemical analysis of CDK4/6 overexpressing and empty vector (E.V.) H1975 EGFR-mutant LUAD CDXs treated with vehicle (0 mg/kg) or osimertinib (2.5-5 mg/kg). Protein expression detected by immunoblotting as indicated. (B) Quantification of p-EGFR immunoblotting shown in (A). (C,D) Growth curves of osimertinib (5 mg/kg) treated CDK4 (C) or CDK6 (D), overexpressing H1975 CDXs compared to empty vector controls (n = 4-6 xenografts per group; error bars representing SEM). (E) Top significantly up- (red) regulated GSEA pathways (n = 3 xenografts per group; p-value calculated as described in methods; NES: Normalized Enrichment Score). (F-H) Representative IHC stained images (F) and quantification (G, H) of Ki-67 from E.V. and CDK4/6 overexpressing H1975 CDXs treated with osimertinib (5 mg/Kg) (n = 3-6 xenografts per group; p-value assessed by one-way ANOVA and Tukey's multiple comparisons test; error bars representing SEM). (I, J) Immunoblotting of replication stress biomarkers p-Rb, TPX2, p-RPA, and p-ATM in CDK4/6 overexpressing H1975 CDXs (I) and quantification (J) versus empty vector (E.V.) controls (error bars representing SEM; following a significant ANOVA result ($p < 0.05$), post-hoc analysis was conducted using Tukey's Honest Significant Difference (HSD) test for pairwise comparisons. Statistical significance is indicated by brackets and p-values, with a threshold of $p < 0.05$). (E.V.: empty vector; CDK4 and CDK6: CDK4 or CDK6 overexpressing CDXs; Veh.: vehicle; Osi.: osimertinib).

Figure 2

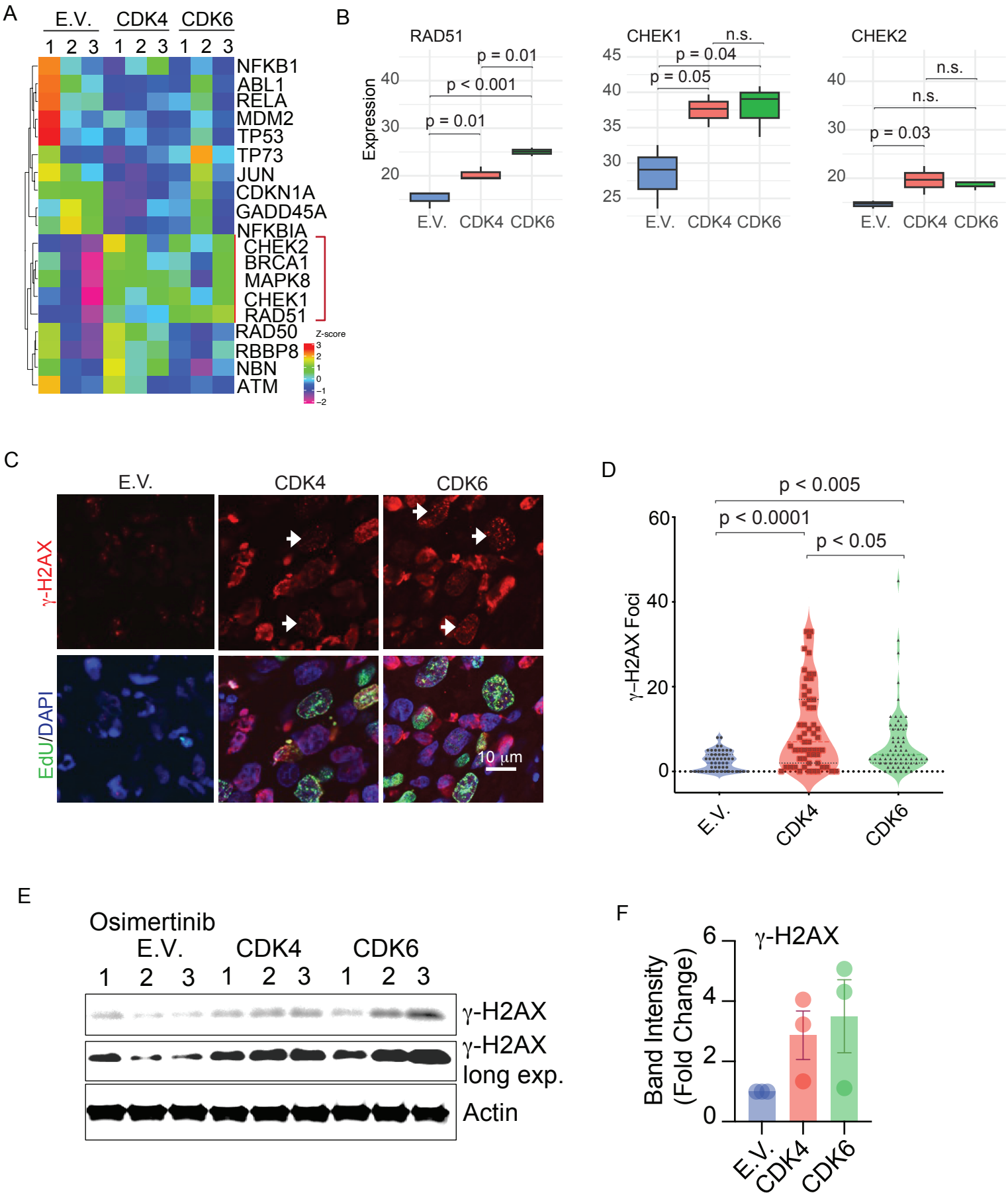
A
E.V.
CDK4
CDK6
1 2 3 1 2 3 1 2 3
NFKB1
ABL1
RELA
MDM2
TP53
TP73
JUN
CDKN1A
GADD45A
NFKBIA
CHEK2
BRCA1
MAPK8
CHEK1
RAD51
RAD50
RBBP8
NBN
ATM
Z-score
3
2
1
0
−1
−2
B
RAD51
Expression
p = 0.01
p < 0.001
p = 0.01
E.V. CDK4 CDK6
CHEK1
n.s.
p = 0.04
p = 0.05
E.V. CDK4 CDK6
CHEK2
n.s.
n.s.
p = 0.03
E.V. CDK4 CDK6
C
E.V.
CDK4
CDK6
γ-H2AX
EdU/DAPI
10 μm
D
p < 0.005
p < 0.0001
p < 0.05
γ–H2AX Foci
E.V.
CDK4
CDK6
E
Osimertinib
E.V.
CDK4
CDK6
1 2 3 1 2 3 1 2 3
γ-H2AX
γ-H2AX
long exp.
Actin
F
γ-H2AX
Band Intensity
(Fold Change)
E.V.
CDK4
CDK6

Figure 2 - CDK4/6 upregulation promotes DNA damage accumulation in EGFRmt LUAD CDXs treated with osimertinib. (A, B) Gene expression profiling of empty vector (E.V.), CDK4, and CDK6 overexpression H1975 CDXs demonstrating statistically significant enrichments in the ATM pathway genes *RAD51*, *CHEK1*, and *CHEK2*, across CDK4/6 overexpressing CDXs compared to E.V. controls (n = 3 xenografts per group; p-value assessed by one-way ANOVA and Tukey's multiple comparisons test). (C, D) Double immunofluorescence stain for γ-H2AX (red) and EdU (green) (C) and quantification of γ-H2AX foci number (D) in EdU positive cells for vehicle-treated H1975 CDXs (white arrows point to double-positive cells; n= 50-100 EdU positive cells per sample, one xenograft per group; p-value calculated with one-way ANOVA and Tukey's multiple comparisons test). (E, F) Biochemical analysis of γ-H2AX expression in CDK4/6 overexpressing H1975 CDXs treated with osimertinib for one week compared to E.V. overexpressing control CDXs (E) and blot's quantification (F) (n = 3 xenografts per group; fold change compared to E.V. controls; error bars representing SEM).
(E.V.: empty vector; CDK4 and CDK6: CDK4 or CDK6 overexpressing CDXs; Veh.: vehicle; Osi.: osimertinib).

Figure 3

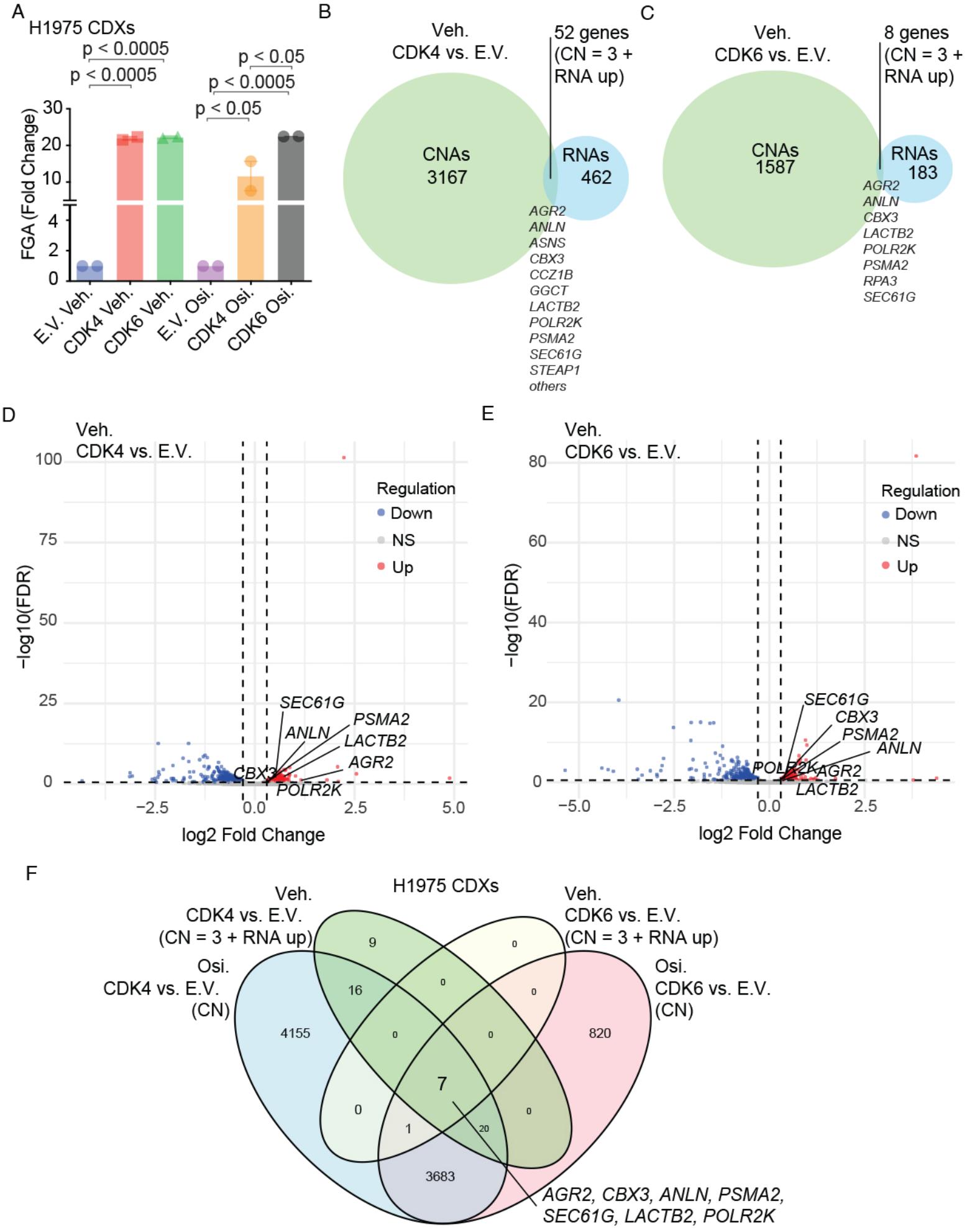
A
H1975 CDXs
p < 0.0005
p < 0.0005
p < 0.05
p < 0.0005
p < 0.05
FGA (Fold Change)
30
20
10
4
2
0
E.V. Veh.
CDK4 Veh.
CDK6 Veh.
E.V. Osi.
CDK4 Osi.
CDK6 Osi.
B
Veh.
CDK4 vs. E.V.
52 genes
(CN = 3 +
RNA up)
CNAs
3167
RNAs
462
AGR2
ANLN
ASNS
CBX3
CCZ1B
GGCT
LACTB2
POLR2K
PSMA2
SEC61G
STEAP1
others
C
Veh.
CDK6 vs. E.V.
8 genes
(CN = 3 +
RNA up)
CNAs
1587
RNAs
183
AGR2
ANLN
CBX3
LACTB2
POLR2K
PSMA2
RPA3
SEC61G
D
Veh.
CDK4 vs. E.V.
Regulation
Down
NS
Up
−log10(FDR)
100
75
50
25
0
SEC61G
PSMA2
ANLN
LACTB2
AGR2
CBX3
POLR2K
−2.5
0.0
2.5
5.0
log2 Fold Change
E
Veh.
CDK6 vs. E.V.
Regulation
Down
NS
Up
−log10(FDR)
80
60
40
20
0
SEC61G
CBX3
PSMA2
ANLN
POLR2K
AGR2
LACTB2
−5.0
−2.5
0.0
2.5
log2 Fold Change
F
H1975 CDXs
Veh.
CDK4 vs. E.V.
(CN = 3 + RNA up)
Veh.
CDK6 vs. E.V.
(CN = 3 + RNA up)
Osi.
CDK4 vs. E.V.
(CN)
Osi.
CDK6 vs. E.V.
(CN)
9
0
16
0
0
4155
0
0
820
7
0
0
1
20
3683
AGR2, CBX3, ANLN, PSMA2,
SEC61G, LACTB2, POLR2K

Figure 3 – Overlap of CDK4/6 upregulated genes with abnormal CN alterations in CDK4/6 overexpressing EGFRmt LUAD CDXs. (A) Fraction of Genome Alterations (FGA) analysis from whole exome sequencing data from osimertinib (5 mg/kg) or vehicle-treated H1975 CDK4/6 overexpressing CDXs compared to empty vector (E.V.) controls (n = 2 xenografts per group; p-value assessed by one-way ANOVA and Tukey's multiple comparisons test; error bars representing SEM). (B, C) Venn diagram illustrating the overlap between genes upregulated in CDK4 (B) or CDK6 (C)-overexpressing CDXs (RNA-seq) and genes with copy number alterations (CNAs) in the vehicle-treated arm (normalized to E.V. CDXs). RNA-seq upregulated genes are shown in sky blue, and CNA-associated genes are shown in green. The intersection indicates genes both transcriptionally upregulated and genomically altered. (D, E) Volcano plot illustrating differential gene expression between CDK4 (D) or CDK6 (E)-overexpressing CDXs vs. E.V. controls. Genes were classified as upregulated (red), downregulated (blue), or not significant (grey) based on log2 fold change (FC) > 0.3 and FDR < 0.3. Selected genes of interest (*AGR2, CBX3, ANLN*, etc.) are annotated. Vertical and horizontal dashed lines represent fold-change and FDR thresholds, respectively. (F) Venn diagram showing the overlap of genes between osimertinib-treated samples (Osi.) and vehicle-treated samples (Veh.), based on upregulated RNA expression (RNA up) and/or copy number alterations (CN = 3; normalized to E.V. CDXs).
(CNAs detected in CDK4 and CDK6 overexpressing CDXs normalized to empty vector control E.V. CDXs in the same treatment group; CDK4: CDK4 overexpressing CDXs; CDK6: CDK6 overexpressing CDXs; for the CNAs analysis, n = 2 xenografts for each group; for the RNAseq experiments, n = 3 xenografts for each group).

Figure 4

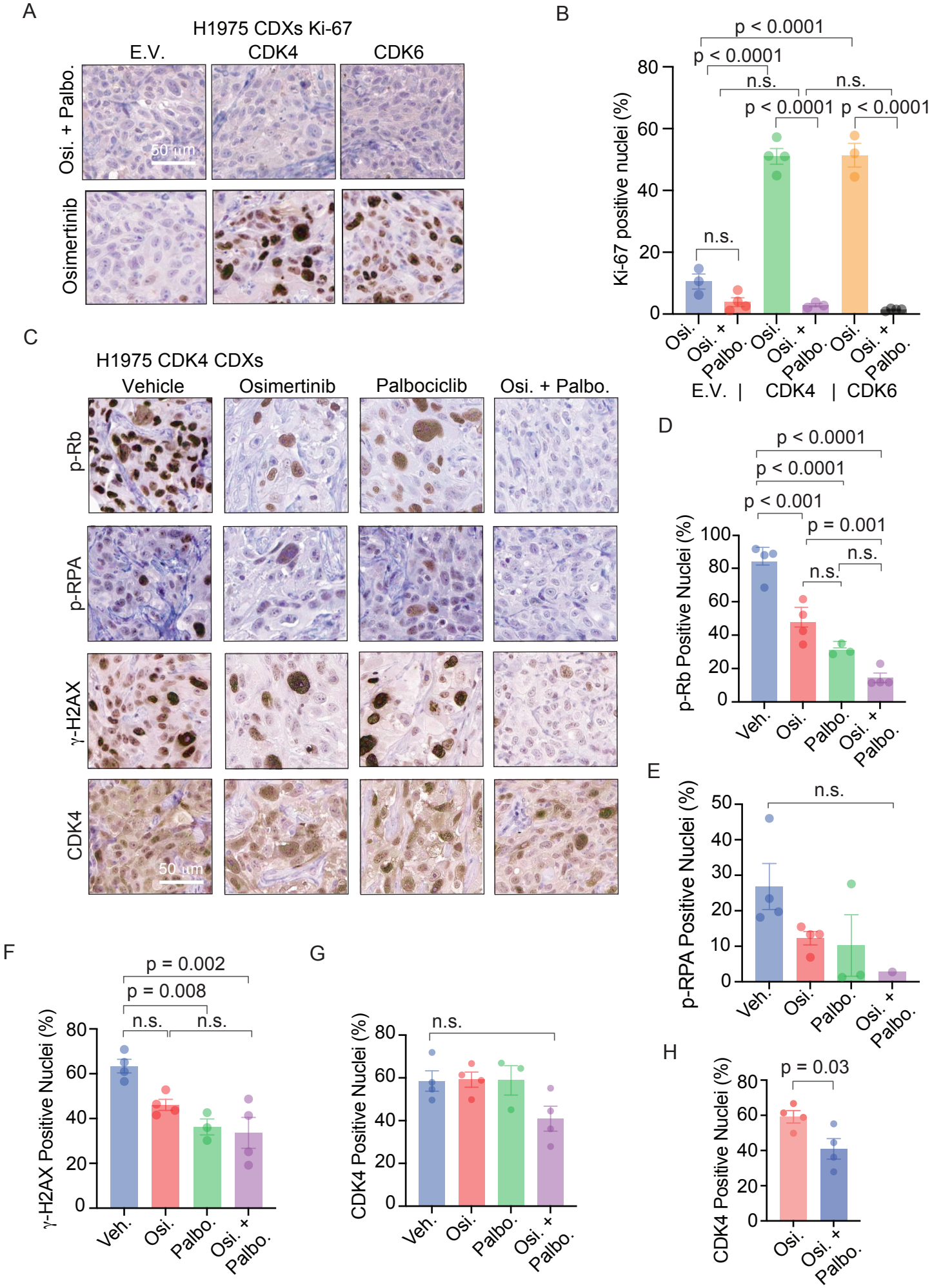
A
H1975 CDXs Ki-67
E.V.
CDK4
CDK6
Osi. + Palbo.
Osimertinib
50 µm
B
Ki-67 positive nuclei (%)
p < 0.0001
p < 0.0001
n.s.
n.s.
p < 0.0001
p < 0.0001
n.s.
Osi.
Osi. + Palbo.
E.V. | CDK4 | CDK6
C
H1975 CDK4 CDXs
Vehicle
Osimertinib
Palbociclib
Osi. + Palbo.
p-Rb
p-RPA
γ-H2AX
CDK4
50 µm
D
p-Rb Positive Nuclei (%)
p < 0.0001
p < 0.0001
p < 0.001
p = 0.001
n.s.
n.s.
Veh.
Osi.
Palbo.
Osi. + Palbo.
E
p-RPA Positive Nuclei (%)
n.s.
F
γ-H2AX Positive Nuclei (%)
p = 0.002
p = 0.008
n.s.
n.s.
G
CDK4 Positive Nuclei (%)
n.s.
H
CDK4 Positive Nuclei (%)
p = 0.03

Figure 4 - Combination therapy with EGFR and CDK4/6 inhibitors suppresses tumor growth and decreases replication stress and genomic instability in CDK4/6 overexpressing EGFRmt LUAD CDXs.

(A, B) Representative Ki-67 IHC stained tumor sections (A) and quantification (B) from E.V. and CDK4/6 overexpressing H1975 CDXs treated with osimertinib (5 mg/kg) or combinatorial treatment with palbociclib (100 mg/kg) (n = 3-4 xenografts per group; p-value assessed by one-way ANOVA and Tukey's multiple comparisons test; error bars representing SEM). (C-H) Representative IHC stained tumor sections (C) and quantification of p-Rb (D), p-RPA (E), γ-H2AX (F), and CDK4 (G, H) from CDK4 overexpressing H1975 CDXs treated with osimertinib (5 mg/kg) and combinatorial treatments with palbociclib (100 mg/kg) (n = 3-4 xenografts per group for Ki-67, p-Rb, p-RPA, γ-H2AX, p-RPA IHC stains; n = 1 for p-RPA in the combinatorial treatment group due to high necrosis in the tissues; p-value assessed by one-way ANOVA and Tukey's multiple comparisons tests and Student's T-test; error bars representing SEM).

(E.V.: empty vector; CDK4: CDK4 overexpressing CDXs; CDK6: CDK6 overexpressing CDXs; Veh.: vehicle; Palbo.: palbociclib; Osi.: osimertinib; p-value assessed by one-way ANOVA and Tukey's multiple comparisons test; error bars representing SEM).

Figure 5

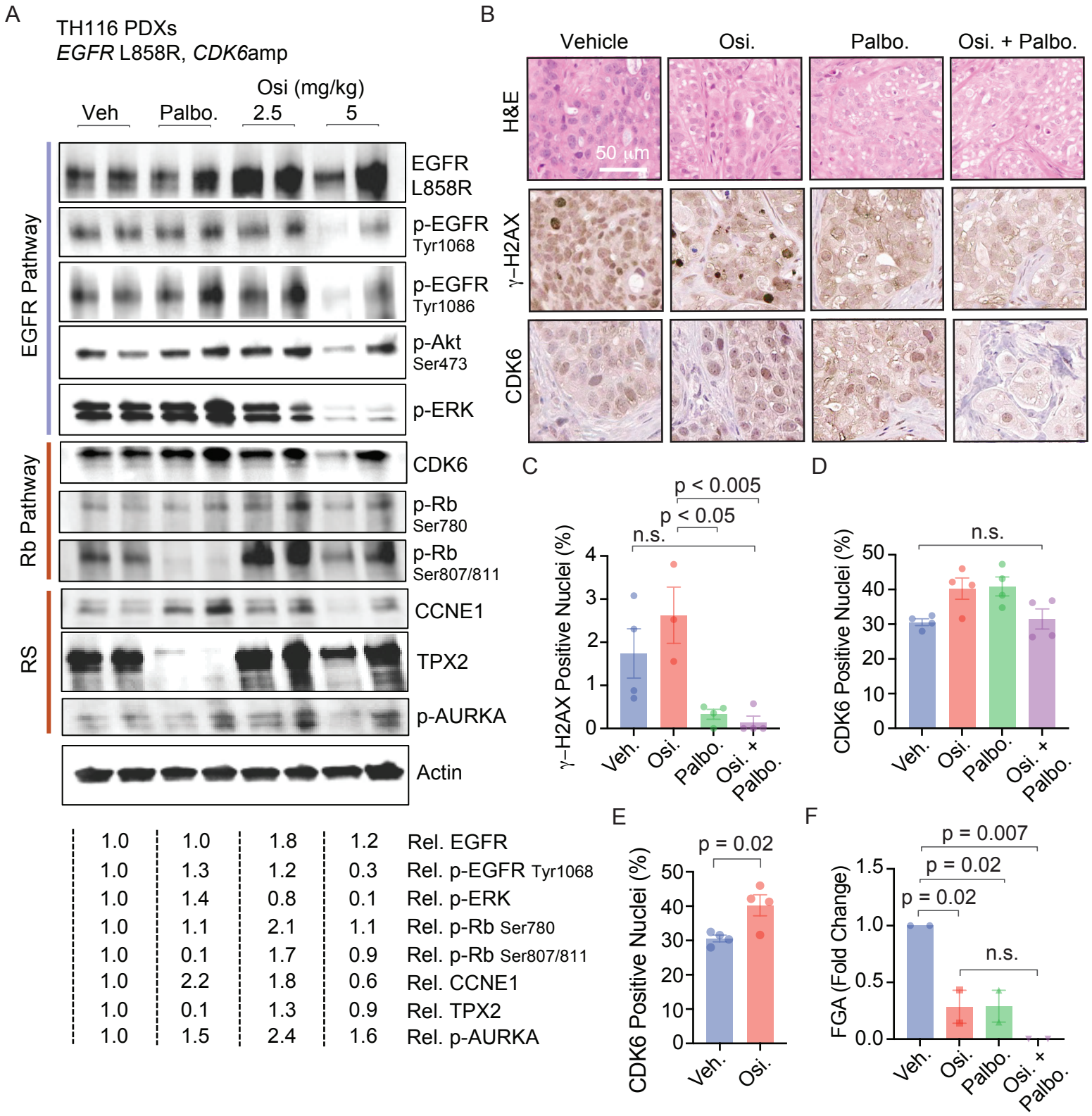

1.0	1.0	1.8	1.2	Rel. EGFR
1.0	1.3	1.2	0.3	Rel. p-EGFR Tyr1068
1.0	1.4	0.8	0.1	Rel. p-ERK
1.0	1.1	2.1	1.1	Rel. p-Rb Ser780
1.0	0.1	1.7	0.9	Rel. p-Rb Ser807/811
1.0	2.2	1.8	0.6	Rel. CCNE1
1.0	0.1	1.3	0.9	Rel. TPX2
1.0	1.5	2.4	1.6	Rel. p-AURKA

Figure 5 - Combination therapy with EGFR and CDK4/6 inhibitors decreases replication stress and genomic instability in a *CDK6*amp, EGFRmt primary LUAD PDXs.

(A) Immunoblotting with quantification for EGFR pathway, CDK6-Rb pathway, and replication stress biomarkers CCNE1, TPX2, and p-AURKA from TH116 (EGFR L8585, *CDK6amp)* primary patient-derived xenografts (PDXs), treated with vehicle, palbociclib (150 mg/kg) or osimertinib (5 mg/kg); normalized quantification of the level of a panel of biomarkers provided in the lower panel. (B-E) Representative hematoxylin/eosin, γ-H2AX, and CDK6 IHC stained tumor sections (B) and quantification (C-E) using tissues from TH116 PDXs (n = 4 xenografts per group; Student T-test). (F) FGA analysis in TH116 PDXs, treated with vehicle, osimertinib (5 mg/kg), palbociclib (100 mg/kg), or a combination of osimertinib and palbociclib (Osi. + Palbo.) (n = 2 xenografts per group; error bars representing SEM). (Veh.: vehicle; Palbo.: palbociclib; Osi.: osimertinib; p-value assessed by one-way ANOVA and Tukey's multiple comparisons tests; error bars representing SEM).

Figure 6

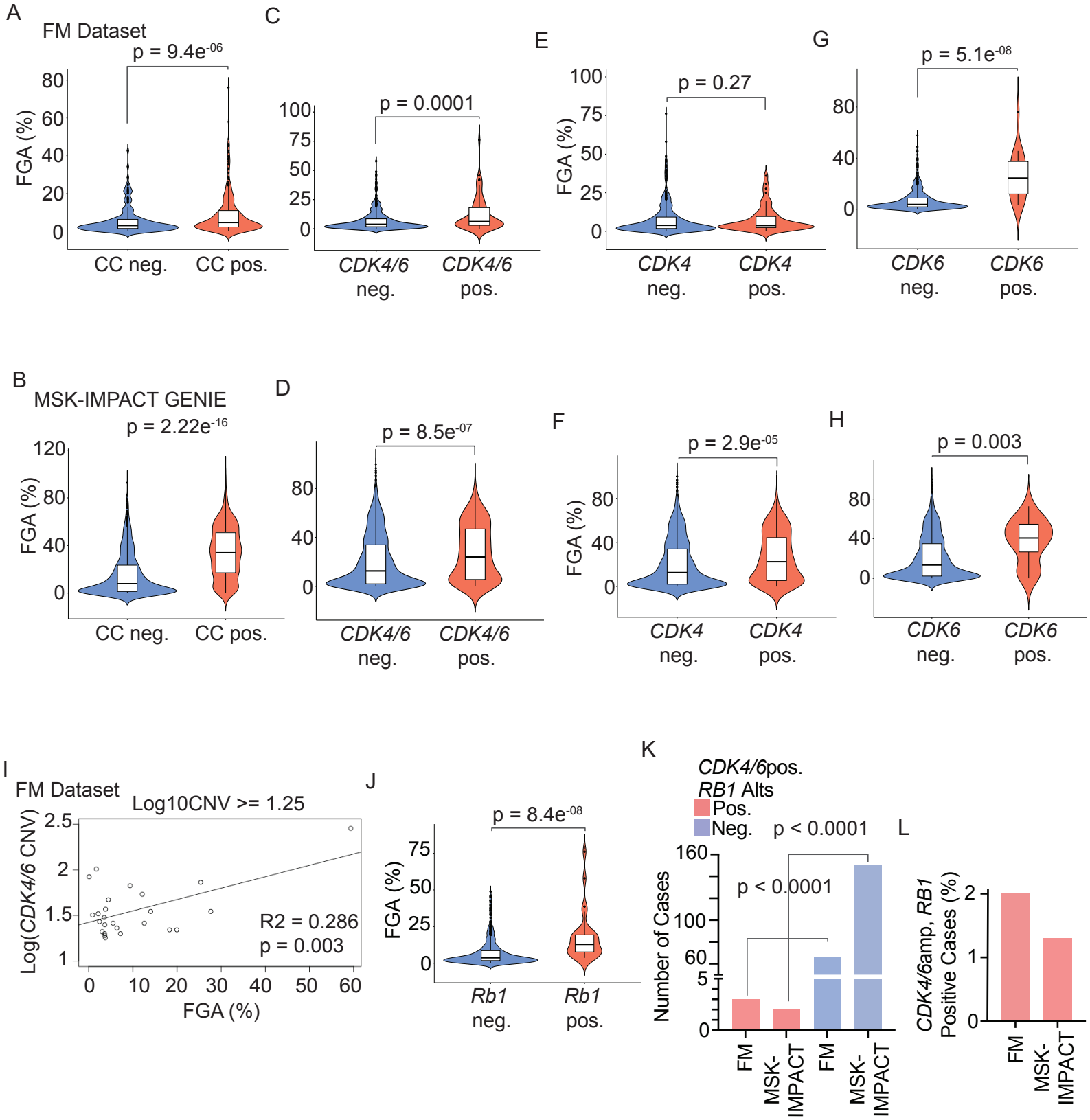
A
FM Dataset
p = 9.4e-06
FGA (%)
CC neg.
CC pos.
C
p = 0.0001
CDK4/6 neg.
CDK4/6 pos.
E
p = 0.27
CDK4 neg.
CDK4 pos.
G
p = 5.1e-08
CDK6 neg.
CDK6 pos.
B
MSK-IMPACT GENIE
p = 2.22e-16
D
p = 8.5e-07
F
p = 2.9e-05
H
p = 0.003
I
FM Dataset
Log10CNV >= 1.25
Log(CDK4/6 CNV)
R2 = 0.286
p = 0.003
FGA (%)
J
p = 8.4e-08
Rb1 neg.
Rb1 pos.
K
CDK4/6pos.
RB1 Alts
Pos.
Neg.
p < 0.0001
p < 0.0001
Number of Cases
FM
MSK-IMPACT
L
CDK4/6amp, RB1 Positive Cases (%)

Figure 6 - Concurrent *EGFRmt* and *CDK4/6* CNAs are associated with an enhanced percentage of genome alterations in LUAD patient tumors.
Fraction of Genome Alterations (FGA) analysis in EGFRmt LUAD using Foundation Medicine (FM) (A) or MSK-Impact GENIE (B) targeted exome sequencing datasets. (A) FGA was compared in tumors harboring concurrent cell cycle CNAs (CC pos.) to tumors negative for such alterations (CC neg.) in the FM (A) and MSK-Impact GENIE datasets (B). (C, D) FGA analysis in EGFRmt tumors stratified by *CDK4/6* CNA status in the FM dataset (C) and MSK-Impact GENIE dataset (D). (E, F) FGA analysis in EGFRmt tumors stratified by *CDK4* CNA status in the FM (E) or MSK-Impact GENIE (F) datasets. (G, H) FGA analysis in EGFRmt tumors stratified by *CDK6* CNA status in the FM (G) or MSK-Impact GENIE (H) datasets. (I) Positive correlation plot showing degrees of *CDK4/6* amplification (y-axis) and corresponding FGA (p-value calculated with F-statistics) (FM Dataset; each dot representing one *CDK4/6* pos. tumor). (J) FGA analysis with FM dataset comparing *RB1* alteration positive versus *RB1* alteration negative EGFRmt LUAD cases. (K, L) Mutual exclusivity analysis (K) and percentage of cases (L) carrying concurrent *CDK4/6* amp and *RB1* gene alterations (SNVs and CNAs) in EGFRmt tumors from Foundation Medicine (FM) or MSK-Impact GENIE targeted exome sequencing (p-value calculated with Fisher's test).
(FGA boxplots included in violin plots represent the interquartile range, lower quartile 25%, median, and upper quartile 75%; p-value calculated with Wilcoxon test).

Figure 7

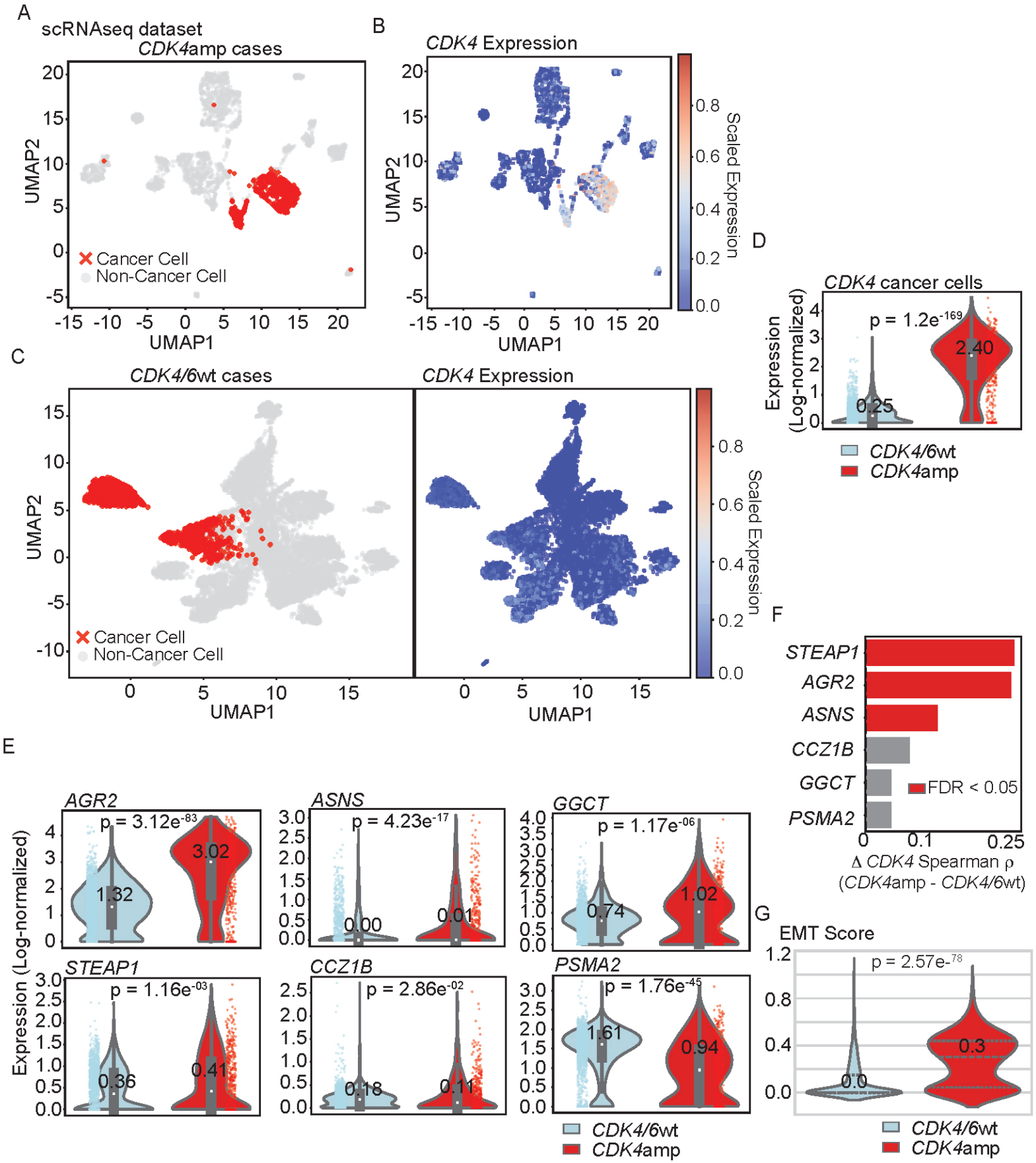
A
scRNAseq dataset
CDK4amp cases
UMAP2
UMAP1
Cancer Cell
Non-Cancer Cell
B
CDK4 Expression
Scaled Expression
C
CDK4/6wt cases
CDK4 Expression
D
CDK4 cancer cells
Expression (Log-normalized)
p = 1.2e-169
2.40
0.25
CDK4/6wt
CDK4amp
E
AGR2
p = 3.12e-83
3.02
1.32
ASNS
p = 4.23e-17
0.00
0.01
GGCT
p = 1.17e-06
1.02
0.74
STEAP1
p = 1.16e-03
0.36
0.41
CCZ1B
p = 2.86e-02
0.18
0.11
PSMA2
p = 1.76e-45
1.61
0.94
Expression (Log-normalized)
CDK4/6wt
CDK4amp
F
STEAP1
AGR2
ASNS
CCZ1B
GGCT
PSMA2
FDR < 0.05
Δ CDK4 Spearman ρ
(CDK4amp - CDK4/6wt)
G
EMT Score
p = 2.57e-78
0.0
0.3
CDK4/6wt
CDK4amp

Figure 7 – Transcriptional changes associated with *CDK4*amp in EGFRmt LUAD cancer cells from patient biopsies.

(A) UMAP visualization of single-cell RNA-seq data from *CDK4*amp, EGFRmt LUAD clinical clinical samples (n = 3), with cancer cells annotated in red based on inferCNV inference. (B) UMAP showing high *CDK4* expression in *CDK4*amp tumor cells, demonstrating localization of CDK4 elevated expression to cancer cells. (C) UMAP visualization of single-cell RNA-seq data from *CDK4/6*wt EGFRmt LUAD clinical samples (n = 11, left scatterplot) and UMAP showing a low degree of *CDK4* expression across *CDK4/6*wt tumor cells (right scatterplot). (D) Violin plots comparing *CDK4* expression in cancer cells from *CDK4*amp (n =3) versus *CDK4/6*wt (n = 11) tumors, showing significantly higher *CDK4* expression in *CDK4*amp cases. (E) Violin plots pointing to *AGR2*, *STEAP1*, *GGCT*, and *ASNS* expression in cancer cells as significantly upregulated in *CDK4*amp versus *CDK4/6*wt tumors. (F) Difference in Spearman correlation of gene expression with *CDK4* gene expression between single cancer cells from *CDK4*amp (n = 483) and *CDK4/6*wt (n = 3188) EGFR-mutant LUAD patients ($\Delta\rho$). P-values were calculated by comparing Fisher z-transformed correlations using a z-test, then adjusted for multiple testing using the False Discovery Rate (FDR). Bars in red indicate genes with significant differences after FDR correction (FDR < 0.05); gray bars are not significant. (G) Violin plot comparing epithelial-mesenchymal transition (EMT) scores in single cancer cells from *CDK4*amp (n = 483) and *CDK4/6*wt (n = 3188) EGFR-mutant LUAD patients. EMT scores were calculated as the mean expression of canonical EMT markers (*VIM*, *ZEB1*, *SNAI1*, *TWIST1*, *CDH2*, and *FN1*). Medians are indicated above each violin. Statistical comparison was performed using a two-sided Mann–Whitney U test.

Figure 8

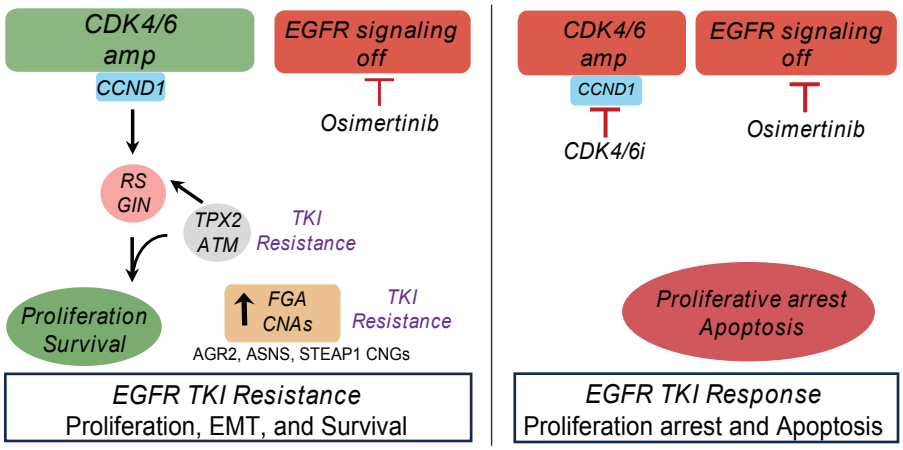
CDK4/6 amp
CCND1
EGFR signaling off
Osimertinib
RS GIN
TPX2 ATM
TKI Resistance
Proliferation Survival
FGA CNAs
TKI Resistance
AGR2, ASNS, STEAP1 CNGs
EGFR TKI Resistance
Proliferation, EMT, and Survival
CDK4/6 amp
CCND1
CDK4/6i
EGFR signaling off
Osimertinib
Proliferative arrest Apoptosis
EGFR TKI Response
Proliferation arrest and Apoptosis

Figure 8 – Model of the effects of *CDK4* or *CDK6* amplification in EGFRmt LUAD. (Left) Schematic model illustrating the impact of *CDK4* or *CDK6* amplification in EGFRmt LUAD. In *CDK4*amp or *CDK6*amp tumors, Rb phosphorylation persists despite EGFR TKI treatment, leading to continued proliferation, accumulation of replication stress (RS) and genomic instability (GIN), and activation of TKI resistance mechanisms (e.g., TPX2/AURKA, ATM). This promotes an increased fraction of genome altered (FGA) and genomic and transcriptional upregulation of tumor promoting genes (e.g., *AGR2*, *ASNS*, *STEAP1*), and epithelial to mesenchymal transition (EMT) contributing to EGFR TKI resistance. (Right) Co-treatment with a CDK4/6 inhibitor (e.g. palbociclib or abemaciclib restores G1/S checkpoint control, reduces proliferation, and induces apoptosis, leading to tumor regression.